Measurement of CP observables in B±-->DCPK ± decays and constraints on the CKM angle gamma

Measurement of CP observables in $B^{\pm} \rightarrow D_{CP}K^{\pm}$ decays and constraints on the CKM angle γ

P. del Amo Sanchez,[1] J. P. Lees,[1] V. Poireau,[1] E. Prencipe,[1] V. Tisserand,[1] J. Garra Tico,[2] E. Grauges,[2] M. Martinelli,[3a,3b] A. Palano,[3b,3b] M. Pappagallo,[3a,3b] G. Eigen,[4] B. Stugu,[4] L. Sun,[4] M. Battaglia,[5] D. N. Brown,[5] B. Hooberman,[5] L. T. Kerth,[5] Yu. G. Kolomensky,[5] G. Lynch,[5] I. L. Osipenkov,[5] T. Tanabe,[5] C. M. Hawkes,[6] A. T. Watson,[6] H. Koch,[7] T. Schroeder,[7] D. J. Asgeirsson,[8] C. Hearty,[8] T. S. Mattison,[8] J. A. McKenna,[8] A. Khan,[9] A. Randle-Conde,[9] V. E. Blinov,[10] A. R. Buzykaev,[10] V. P. Druzhinin,[10] V. B. Golubev,[10] A. P. Onuchin,[10] S. I. Serednyakov,[10] Yu. I. Skovpen,[10] E. P. Solodov,[10] K. Yu. Todyshev,[10] A. N. Yushkov,[10] M. Bondioli,[11] S. Curry,[11] D. Kirkby,[11] A. J. Lankford,[11] M. Mandelkern,[11] E. C. Martin,[11] D. P. Stoker,[11] H. Atmacan,[12] J. W. Gary,[12] F. Liu,[12] O. Long,[12] G. M. Vitug,[12] C. Campagnari,[13] T. M. Hong,[13] D. Kovalskyi,[13] J. D. Richman,[13] A. M. Eisner,[14] C. A. Heusch,[14] J. Kroseberg,[14] W. S. Lockman,[14] A. J. Martinez,[14] T. Schalk,[14] B. A. Schumm,[14] A. Seiden,[14] L. O. Winstrom,[14] C. H. Cheng,[15] D. A. Doll,[15] B. Echenard,[15] D. G. Hitlin,[15] P. Ongmongkolkul,[15] F. C. Porter,[15] A. Y. Rakitin,[15] R. Andreassen,[16] M. S. Dubrovin,[16] G. Mancinelli,[16] B. T. Meadows,[16] M. D. Sokoloff,[16] P. C. Bloom,[17] W. T. Ford,[17] A. Gaz,[17] M. Nagel,[17] U. Nauenberg,[17] J. G. Smith,[17] S. R. Wagner,[17] R. Ayad,[18,*] W. H. Toki,[18] H. Jasper,[19] T. M. Karbach,[19] J. Merkel,[19] A. Petzold,[19] B. Spaan,[19] K. Wacker,[19] M. J. Kobel,[20] K. R. Schubert,[20] R. Schwierz,[20] D. Bernard,[21] M. Verderi,[21] P. J. Clark,[22] S. Playfer,[22] J. E. Watson,[22] M. Andreotti,[23a,23b] D. Bettoni,[23a] C. Bozzi,[23a] R. Calabrese,[23a,23b] A. Cecchi,[23a,23b] G. Cibinetto,[23a,23b] E. Fioravanti,[23a,23b] P. Franchini,[23a,23b] E. Luppi,[23a,23b] M. Munerato,[23a,23b] M. Negrini,[23a,23b] A. Petrella,[23a,23b] L. Piemontese,[23a] R. Baldini-Ferroli,[24] A. Calcaterra,[24] R. de Sangro,[24] G. Finocchiaro,[24] M. Nicolaci,[24] S. Pacetti,[24] P. Patteri,[24] I. M. Peruzzi,[24,†] M. Piccolo,[24] M. Rama,[24] A. Zallo,[24] R. Contri,[25a,25b] E. Guido,[25a,25b] M. Lo Vetere,[25a,25b] M. R. Monge,[25a,25b] S. Passaggio,[25a] C. Patrignani,[25a,25b] E. Robutti,[25a] S. Tosi,[25a,25b] B. Bhuyan,[26] V. Prasad,[26] C. L. Lee,[27] M. Morii,[27] A. Adametz,[28] J. Marks,[28] S. Schenk,[28] U. Uwer,[28] F. U. Bernlochner,[29] M. Ebert,[29] H. M. Lacker,[29] T. Lueck,[29] A. Volk,[29] P. D. Dauncey,[30] M. Tibbetts,[30] P. K. Behera,[31] U. Mallik,[31] C. Chen,[32] J. Cochran,[32] H. B. Crawley,[32] L. Dong,[32] W. T. Meyer,[32] S. Prell,[32] E. I. Rosenberg,[32] A. E. Rubin,[32] Y. Y. Gao,[33] A. V. Gritsan,[33] Z. J. Guo,[33] N. Arnaud,[34] M. Davier,[34] D. Derkach,[34] J. Firmino da Costa,[34] G. Grosdidier,[34] F. Le Diberder,[34] A. M. Lutz,[34] B. Malaescu,[34] A. Perez,[34] P. Roudeau,[34] M. H. Schune,[34] J. Serrano,[34] V. Sordini,[34,‡] A. Stocchi,[34] L. Wang,[34] G. Wormser,[34] D. J. Lange,[35] D. M. Wright,[35] I. Bingham,[36] C. A. Chavez,[36] J. P. Coleman,[36] J. R. Fry,[36] E. Gabathuler,[36] R. Gamet,[36] D. E. Hutchcroft,[36] D. J. Payne,[36] C. Touramanis,[36] A. J. Bevan,[37] F. Di Lodovico,[37] R. Sacco,[37] M. Sigamani,[37] G. Cowan,[38] S. Paramesvaran,[38] A. C. Wren,[38] D. N. Brown,[39] C. L. Davis,[39] A. G. Denig,[40] M. Fritsch,[40] W. Gradl,[40] A. Hafner,[40] K. E. Alwyn,[41] D. Bailey,[41] R. J. Barlow,[41] G. Jackson,[41] G. D. Lafferty,[41] T. J. West,[41] J. Anderson,[42] R. Cenci,[42] A. Jawahery,[42] D. A. Roberts,[42] G. Simi,[42] J. M. Tuggle,[42] C. Dallapiccola,[43] E. Salvati,[43] R. Cowan,[44] D. Dujmic,[44] P. H. Fisher,[44] G. Sciolla,[44] M. Zhao,[44] D. Lindemann,[45] P. M. Patel,[45] S. H. Robertson,[45] M. Schram,[45] P. Biassoni,[46a,46b] A. Lazzaro,[46a,46b] V. Lombardo,[46a] F. Palombo,[46a,46b] S. Stracka,[46a,46b] L. Cremaldi,[47] R. Godang,[47,§] R. Kroeger,[47] P. Sonnek,[47] D. J. Summers,[47] X. Nguyen,[48] M. Simard,[48] P. Taras,[48] G. De Nardo,[49a,49b] D. Monorchio,[49a,49b] G. Onorato,[49a,49b] C. Sciacca,[49a,49b] G. Raven,[50] H. L. Snoek,[50] C. P. Jessop,[51] K. J. Knoepfel,[51] J. M. LoSecco,[51] W. F. Wang,[51] L. A. Corwin,[52] K. Honscheid,[52] R. Kass,[52] J. P. Morris,[52] A. M. Rahimi,[52] N. L. Blount,[53] J. Brau,[53] R. Frey,[53] O. Igonkina,[53] J. A. Kolb,[53] R. Rahmat,[53] N. B. Sinev,[53] D. Strom,[53] J. Strube,[53] E. Torrence,[53] G. Castelli,[54a,54b] E. Feltresi,[54a,54b] N. Gagliardi,[54a,54b] M. Margoni,[54a,54b] M. Morandin,[54a] M. Posocco,[54a] M. Rotondo,[54a] F. Simonetto,[54a,54b] R. Stroili,[54a,54b] E. Ben-Haim,[55] G. R. Bonneaud,[55] H. Briand,[55] G. Calderini,[55] J. Chauveau,[55] O. Hamon,[55] Ph. Leruste,[55] G. Marchiori,[55] J. Ocariz,[55] J. Prendki,[55] S. Sitt,[55] M. Biasini,[56a,56b] E. Manoni,[56a,56b] A. Rossi,[56a,56b] C. Angelini,[57a,57b] G. Batignani,[57a,57b] S. Bettarini,[57a,57b] M. Carpinelli,[57a,57b,‖] G. Casarosa,[57a,57b] A. Cervelli,[57a,57b] F. Forti,[57a,57b] M. A. Giorgi,[57a,57b] A. Lusiani,[57a,57c] N. Neri,[57a,57b] E. Paoloni,[57a,57b] G. Rizzo,[57a,57b] J. J. Walsh,[57a] D. Lopes Pegna,[58] C. Lu,[58] J. Olsen,[58] A. J. S. Smith,[58] A. V. Telnov,[58] F. Anulli,[59a] E. Baracchini,[59a,59b] G. Cavoto,[59a] R. Faccini,[59a,59b] F. Ferrarotto,[59a] F. Ferroni,[59a,59b] M. Gaspero,[59a,59b] L. Li Gioi,[59a] M. A. Mazzoni,[59a] G. Piredda,[59a] F. Renga,[59a,59b] T. Hartmann,[60] T. Leddig,[60] H. Schröder,[60] R. Waldi,[60] T. Adye,[61] B. Franek,[61] E. O. Olaiya,[61] F. F. Wilson,[61] S. Emery,[62] G. Hamel de Monchenault,[62] G. Vasseur,[62] Ch. Yèche,[62] M. Zito,[62] M. T. Allen,[63] D. Aston,[63] D. J. Bard,[63] R. Bartoldus,[63] J. F. Benitez,[63] C. Cartaro,[63] M. R. Convery,[63] J. Dorfan,[63] G. P. Dubois-Felsmann,[63] W. Dunwoodie,[63] R. C. Field,[63] M. Franco Sevilla,[63] B. G. Fulsom,[63] A. M. Gabareen,[63] M. T. Graham,[63] P. Grenier,[63] C. Hast,[63] W. R. Innes,[63] M. H. Kelsey,[63] H. Kim,[63] P. Kim,[63] M. L. Kocian,[63] D. W. G. S. Leith,[63] S. Li,[63] B. Lindquist,[63] S. Luitz,[63] V. Luth,[63] H. L. Lynch,[63] D. B. MacFarlane,[63] H. Marsiske,[63] D. R. Muller,[63] H. Neal,[63] S. Nelson,[63] C. P. O'Grady,[63] I. Ofte,[63] M. Perl,[63] T. Pulliam,[63] B. N. Ratcliff,[63] A. Roodman,[63]

A. A. Salnikov,[63] V. Santoro,[63] R. H. Schindler,[63] J. Schwiening,[63] A. Snyder,[63] D. Su,[63] M. K. Sullivan,[63] S. Sun,[63] K. Suzuki,[63] J. M. Thompson,[63] J. Va'vra,[63] A. P. Wagner,[63] M. Weaver,[63] C. A. West,[63] W. J. Wisniewski,[63] M. Wittgen,[63] D. H. Wright,[63] H. W. Wulsin,[63] A. K. Yarritu,[63] C. C. Young,[63] V. Ziegler,[63] X. R. Chen,[64] W. Park,[64] M. V. Purohit,[64] R. M. White,[64] J. R. Wilson,[64] S. J. Sekula,[65] M. Bellis,[66] P. R. Burchat,[66] A. J. Edwards,[66] T. S. Miyashita,[66] S. Ahmed,[67] M. S. Alam,[67] J. A. Ernst,[67] B. Pan,[67] M. A. Saeed,[67] S. B. Zain,[67] N. Guttman,[68] A. Soffer,[68] P. Lund,[69] S. M. Spanier,[69] R. Eckmann,[70] J. L. Ritchie,[70] A. M. Ruland,[70] C. J. Schilling,[70] R. F. Schwitters,[70] B. C. Wray,[70] J. M. Izen,[71] X. C. Lou,[71] F. Bianchi,[72a,72b] D. Gamba,[72a,72b] M. Pelliccioni,[72a,72b] M. Bomben,[73a,73b] L. Lanceri,[73a,73b] L. Vitale,[73a,73b] N. Lopez-March,[74] F. Martinez-Vidal,[74] D. A. Milanes,[74] A. Oyanguren,[74] J. Albert,[75] Sw. Banerjee,[75] H. H. F. Choi,[75] K. Hamano,[75] G. J. King,[75] R. Kowalewski,[75] M. J. Lewczuk,[75] I. M. Nugent,[75] J. M. Roney,[75] R. J. Sobie,[75] T. J. Gershon,[76] P. F. Harrison,[76] T. E. Latham,[76] E. M. T. Puccio,[76] H. R. Band,[77] S. Dasu,[77] K. T. Flood,[77] Y. Pan,[77] R. Prepost,[77] C. O. Vuosalo,[77] and S. L. Wu[77]

[1]*Laboratoire d'Annecy-le-Vieux de Physique des Particules (LAPP),
Université de Savoie, CNRS/IN2P3, F-74941 Annecy-Le-Vieux, France*
[2]*Universitat de Barcelona, Facultat de Fisica, Departament ECM, E-08028 Barcelona, Spain*
[3a]*INFN Sezione di Bari, I-70126 Bari, Italy;*
[3b]*Dipartimento di Fisica, Università di Bari, I-70126 Bari, Italy*
[4]*University of Bergen, Institute of Physics, N-5007 Bergen, Norway*
[5]*Lawrence Berkeley National Laboratory and University of California, Berkeley, California 94720, USA*
[6]*University of Birmingham, Birmingham, B15 2TT, United Kingdom*
[7]*Ruhr Universität Bochum, Institut für Experimentalphysik 1, D-44780 Bochum, Germany*
[8]*University of British Columbia, Vancouver, British Columbia, Canada V6T 1Z1*
[9]*Brunel University, Uxbridge, Middlesex UB8 3PH, United Kingdom*
[10]*Budker Institute of Nuclear Physics, Novosibirsk 630090, Russia*
[11]*University of California at Irvine, Irvine, California 92697, USA*
[12]*University of California at Riverside, Riverside, California 92521, USA*
[13]*University of California at Santa Barbara, Santa Barbara, California 93106, USA*
[14]*University of California at Santa Cruz, Institute for Particle Physics, Santa Cruz, California 95064, USA*
[15]*California Institute of Technology, Pasadena, California 91125, USA*
[16]*University of Cincinnati, Cincinnati, Ohio 45221, USA*
[17]*University of Colorado, Boulder, Colorado 80309, USA*
[18]*Colorado State University, Fort Collins, Colorado 80523, USA*
[19]*Technische Universität Dortmund, Fakultät Physik, D-44221 Dortmund, Germany*
[20]*Technische Universität Dresden, Institut für Kern- und Teilchenphysik, D-01062 Dresden, Germany*
[21]*Laboratoire Leprince-Ringuet, CNRS/IN2P3, Ecole Polytechnique, F-91128 Palaiseau, France*
[22]*University of Edinburgh, Edinburgh EH9 3JZ, United Kingdom*
[23a]*INFN Sezione di Ferrara, I-44100 Ferrara, Italy;*
[23b]*Dipartimento di Fisica, Università di Ferrara, I-44100 Ferrara, Italy*
[24]*INFN Laboratori Nazionali di Frascati, I-00044 Frascati, Italy*
[25a]*INFN Sezione di Genova, I-16146 Genova, Italy;*
[25b]*Dipartimento di Fisica, Università di Genova, I-16146 Genova, Italy*
[26]*Indian Institute of Technology Guwahati, Guwahati, Assam, 781 039, India*
[27]*Harvard University, Cambridge, Massachusetts 02138, USA*
[28]*Universität Heidelberg, Physikalisches Institut, Philosophenweg 12, D-69120 Heidelberg, Germany*
[29]*Humboldt-Universität zu Berlin, Institut für Physik, Newtonstr. 15, D-12489 Berlin, Germany*
[30]*Imperial College London, London, SW7 2AZ, United Kingdom*
[31]*University of Iowa, Iowa City, Iowa 52242, USA*
[32]*Iowa State University, Ames, Iowa 50011-3160, USA*
[33]*Johns Hopkins University, Baltimore, Maryland 21218, USA*
[34]*Laboratoire de l'Accélérateur Linéaire, IN2P3/CNRS et Université Paris-Sud 11,
Centre Scientifique d'Orsay, B. P. 34, F-91898 Orsay Cedex, France*
[35]*Lawrence Livermore National Laboratory, Livermore, California 94550, USA*
[36]*University of Liverpool, Liverpool L69 7ZE, United Kingdom*
[37]*Queen Mary, University of London, London, E1 4NS, United Kingdom*
[38]*University of London, Royal Holloway and Bedford New College, Egham, Surrey TW20 0EX, United Kingdom*
[39]*University of Louisville, Louisville, Kentucky 40292, USA*
[40]*Johannes Gutenberg-Universität Mainz, Institut für Kernphysik, D-55099 Mainz, Germany*
[41]*University of Manchester, Manchester M13 9PL, United Kingdom*
[42]*University of Maryland, College Park, Maryland 20742, USA*

[43]*University of Massachusetts, Amherst, Massachusetts 01003, USA*
[44]*Massachusetts Institute of Technology, Laboratory for Nuclear Science, Cambridge, Massachusetts 02139, USA*
[45]*McGill University, Montréal, Québec, Canada H3A 2T8*
[46a]*INFN Sezione di Milano, I-20133 Milano, Italy;*
[46b]*Dipartimento di Fisica, Università di Milano, I-20133 Milano, Italy*
[47]*University of Mississippi, University, Mississippi 38677, USA*
[48]*Université de Montréal, Physique des Particules, Montréal, Québec, Canada H3C 3J7*
[49a]*INFN Sezione di Napoli, I-80126 Napoli, Italy;*
[49b]*Dipartimento di Scienze Fisiche, Università di Napoli Federico II, I-80126 Napoli, Italy*
[50]*NIKHEF, National Institute for Nuclear Physics and High Energy Physics, NL-1009 DB Amsterdam, The Netherlands*
[51]*University of Notre Dame, Notre Dame, Indiana 46556, USA*
[52]*Ohio State University, Columbus, Ohio 43210, USA*
[53]*University of Oregon, Eugene, Oregon 97403, USA*
[54a]*INFN Sezione di Padova, I-35131 Padova, Italy;*
[54b]*Dipartimento di Fisica, Università di Padova, I-35131 Padova, Italy*
[55]*Laboratoire de Physique Nucléaire et de Hautes Energies, IN2P3/CNRS,*
Université Pierre et Marie Curie-Paris6, Université Denis Diderot-Paris7, F-75252 Paris, France
[56a]*INFN Sezione di Perugia, I-06100 Perugia, Italy;*
[56b]*Dipartimento di Fisica, Università di Perugia, I-06100 Perugia, Italy*
[57a]*INFN Sezione di Pisa, I-56127 Pisa, Italy;*
[57b]*Dipartimento di Fisica, Università di Pisa, I-56127 Pisa, Italy;*
[57c]*Scuola Normale Superiore di Pisa, I-56127 Pisa, Italy*
[58]*Princeton University, Princeton, New Jersey 08544, USA*
[59a]*INFN Sezione di Roma, I-00185 Roma, Italy;*
[59b]*Dipartimento di Fisica, Università di Roma La Sapienza, I-00185 Roma, Italy*
[60]*Universität Rostock, D-18051 Rostock, Germany*
[61]*Rutherford Appleton Laboratory, Chilton, Didcot, Oxon, OX11 0QX, United Kingdom*
[62]*CEA, Irfu, SPP, Centre de Saclay, F-91191 Gif-sur-Yvette, France*
[63]*SLAC National Accelerator Laboratory, Stanford, California 94309 USA*
[64]*University of South Carolina, Columbia, South Carolina 29208, USA*
[65]*Southern Methodist University, Dallas, Texas 75275, USA*
[66]*Stanford University, Stanford, California 94305-4060, USA*
[67]*State University of New York, Albany, New York 12222, USA*
[68]*Tel Aviv University, School of Physics and Astronomy, Tel Aviv, 69978, Israel*
[69]*University of Tennessee, Knoxville, Tennessee 37996, USA*
[70]*University of Texas at Austin, Austin, Texas 78712, USA*
[71]*University of Texas at Dallas, Richardson, Texas 75083, USA*
[72a]*INFN Sezione di Torino, I-10125 Torino, Italy;*
[72b]*Dipartimento di Fisica Sperimentale, Università di Torino, I-10125 Torino, Italy*
[73a]*INFN Sezione di Trieste, I-34127 Trieste, Italy;*
[73b]*Dipartimento di Fisica, Università di Trieste, I-34127 Trieste, Italy*
[74]*IFIC, Universitat de Valencia-CSIC, E-46071 Valencia, Spain*
[75]*University of Victoria, Victoria, British Columbia, Canada V8W 3P6*
[76]*Department of Physics, University of Warwick, Coventry CV4 7AL, United Kingdom*
[77]*University of Wisconsin, Madison, Wisconsin 53706, USA*

Using the entire sample of 467×10^6 $\Upsilon(4S) \to B\bar{B}$ decays collected with the *BABAR* detector at the PEP-II asymmetric-energy *B* factory at the SLAC National Accelerator Laboratory, we perform an analysis of $B^{\pm} \to DK^{\pm}$ decays, using decay modes in which the neutral *D* meson decays to either *CP*-eigenstates or non-*CP*-eigenstates. We measure the partial decay rate charge asymmetries for *CP*-even and *CP*-odd *D* final states to be $A_{CP+} = 0.25 \pm 0.06 \pm 0.02$ and $A_{CP-} = -0.09 \pm 0.07 \pm 0.02$, respectively, where the first error is the statistical and the second is the systematic uncertainty. The parameter A_{CP+} is different from zero with a significance of 3.6 standard deviations, constituting evidence for direct *CP* violation. We

[*]Now at Temple University, Philadelphia, Pennsylvania 19122, USA
[†]Also with Università di Perugia, Dipartimento di Fisica, Perugia, Italy
[‡]Also with Università di Roma La Sapienza, I-00185 Roma, Italy
[§]Now at University of South Alabama, Mobile, Alabama 36688, USA
[‖]Also with Università di Sassari, Sassari, Italy

also measure the ratios of the charged-averaged B partial decay rates in CP and non-CP decays, $R_{CP+} = 1.18 \pm 0.09 \pm 0.05$ and $R_{CP-} = 1.07 \pm 0.08 \pm 0.04$. We infer frequentist confidence intervals for the angle γ of the unitarity triangle, for the strong phase difference δ_B, and for the amplitude ratio r_B, which are related to the $B^- \rightarrow DK^-$ decay amplitude by $r_B e^{i(\delta_B - \gamma)} = A(B^- \rightarrow \bar{D}^0 K^-)/A(B^- \rightarrow D^0 K^-)$. Including statistical and systematic uncertainties, we obtain $0.24 < r_B < 0.45$ ($0.06 < r_B < 0.51$) and, modulo 180°, $11.3° < \gamma < 22.7°$ or $80.8° < \gamma < 99.2°$ or $157.3° < \gamma < 168.7°$ ($7.0° < \gamma < 173.0°$) at the 68% (95%) confidence level.

I. INTRODUCTION

In the standard model (SM) of fundamental particles, CP violation in weak interactions is allowed by a single, irreducible phase in the 3×3 Cabibbo-Kobayashi-Maskawa (CKM) quark flavor-mixing matrix [1,2]. The unitarity of the CKM matrix, V, implies a set of relations among its elements V_{ij}, in particular, the condition $V_{ud}V_{ub}^* + V_{cd}V_{cb}^* + V_{td}V_{tb}^* = 0$, which can be depicted in the complex plane as a "unitarity" triangle, whose sides and angles are related to the magnitudes and phases of the six elements V_{id} and V_{ib}, where $i = u$, c, t. Overconstraining the unitarity triangle by means of precise measurements of all its sides and angles allows tests of whether the CKM mechanism is the correct description of CP violation. Any inconsistencies among the various experimental constraints would reveal effects of physics beyond the standard model.

After a decade of successful operation and a total of about 1.3×10^9 $B\bar{B}$ pairs collected by the *BABAR* and Belle experiments, the three CKM angles have been measured with varied precision. The angle β has been measured with the highest precision, to around 1°, using $B^0 \rightarrow (c\bar{c})K^{(*)0}$ decays. Using a variety of two-body B decays ($B \rightarrow \pi\pi$, $\rho\pi$, $\rho\rho$ and $a_1(1260)\pi$) the angle α has been measured to a precision of around 4°. The angle γ has a relatively large uncertainty, around 14°, compared with α and β. The lack of precision in our knowledge of γ reflects the difficulty in measuring this angle. The uncertainties of the CKM angles quoted in this paragraph are taken from [3].

Several techniques for measuring γ in a theoretically clean way are based on B meson decays to open-charm final states, $D^{(*)0}X_s$ and $\bar{D}^{(*)0}X_s$ ($X_s = K^{(*)\pm}$, $K^{(*)0}$). In these decays, the interference between the $b \rightarrow c\bar{u}s$ and $b \rightarrow u\bar{c}s$ tree amplitudes, when the D^0 and $\bar{D}^0$ decay to a common final state, leads to observables that depend on the relative weak phase γ. The size of the interference also depends on the magnitude of the ratio r_B and the relative strong phase δ_B of the two amplitudes, which cannot be precisely calculated from theory. They can be extracted directly from data by simultaneously reconstructing several related $B \rightarrow DK$ decays. Many methods have been proposed to extract γ from B decays using $D^{(*)}K^{(*)\pm}$ and $D^{(*)}K^{(*)0}$ final states (here and in the following D refers to any admixture of the neutral D^0 meson and its CP-conjugate $\bar{D}^0$). The three methods that have been used most productively to date are the "GLW" method [4,5], based on Cabibbo-suppressed D decays to CP-eigenstates, such as K^+K^- or $K^0_S\pi^0$; the "ADS" method [6,7], where the D is reconstructed in Cabibbo-favored and doubly-Cabibbo-suppressed final states such as $K^{\pm}\pi^{\mp}$; and the "GGSZ" method [8], which studies the Dalitz-plot distribution of the products of D decays to multibody self-conjugate final states, such as $K^0_S\pi^+\pi^-$. A common problem with these methods is the small overall branching fraction of these decays ranging from 5×10^{-6} to 5×10^{-9}. Therefore a precise determination of γ requires a very large data sample. *BABAR* has published several γ related measurements: GLW analyses of $B^{\pm} \rightarrow DK^{\pm}$ [9], $D^*K^{\pm}$ [10] and $DK^{*\pm}$ [11] decays; ADS analyses of $B^{\pm} \rightarrow D^{(*)}K^{\pm}$ [12,13], $DK^{*\pm}$ [11] and $B^0 \rightarrow DK^{*0}$ [14]; and GGSZ analyses of $B^{\pm} \rightarrow D^{(*)}K^{(*)\pm}$ [15,16] and $B^0 \rightarrow DK^{*0}$ decays [17]. To date, the single most precise experimental determination of γ from *BABAR* is $\gamma = (68 \pm 14 \pm 4 \pm 3)°$ and $39° < \gamma < 98°$, obtained from the GGSZ analysis of $B^{\pm} \rightarrow D^{(*)}K^{(*)\pm}$ decays [16]. In this measurement, the first error represents the statistical uncertainty, the second is the experimental systematic uncertainty, and the third reflects the uncertainty on the description of the D Dalitz-plot distributions.

II. GLW ANALYSIS OF $B \rightarrow DK$ DECAYS

In this paper we present the update of the GLW analysis of $B^{\pm} \rightarrow DK^{\pm}$ decays based on the full *BABAR* data set collected near the $\Upsilon(4S)$ resonance. In addition to a 22% increase in statistics of the data sample, this study benefits from other significant improvements compared to our previous result [9]:

(i) More refined charged track reconstruction and particle identification algorithms, with higher purity and efficiency, have been employed;

(ii) The event shape variable $\mathcal{F}$, used to discriminate the signal from the continuum $e^+e^- \rightarrow q\bar{q}$ background (described in detail in Sec. IV) has been removed from the selection criteria and has instead been included in the final fit to the selected B candidates. This allows us to increase the signal efficiency by 40% to 60%. At the same time it provides a larger sample of continuum background

events, thus allowing for the determination of the background properties directly from data (see Sec. V);

(iii) Better kaon/pion separation, which is needed to distinguish $B^\pm \to DK^\pm$ candidates from the 12 times more abundant $B^\pm \to D\pi^\pm$ decays, is achieved through the use of a global likelihood based not only on the Cherenkov angle θ_C reconstructed by the Cherenkov detector, but also on the specific energy loss dE/dx measured by the tracking devices. The inclusion of dE/dx in the likelihood increases the kaon identification efficiency and decreases the pion misidentification both at low momentum and outside of the geometrical acceptance of the Cherenkov detector (which is 10% lower than the acceptance of the tracking devices).

In order to determine γ from $B^\pm \to DK^\pm$ decays with the GLW method, we measure the two direct-*CP*-violating partial decay rate asymmetries,

$$A_{CP\pm} \equiv \frac{\Gamma(B^- \to D_{CP\pm}K^-) - \Gamma(B^+ \to D_{CP\pm}K^+)}{\Gamma(B^- \to D_{CP\pm}K^-) + \Gamma(B^+ \to D_{CP\pm}K^+)}, \quad (1)$$

and the two ratios of charge averaged partial rates using D decays to *CP* and flavor eigenstates,

$$R_{CP\pm} \equiv 2\frac{\Gamma(B^- \to D_{CP\pm}K^-) + \Gamma(B^+ \to D_{CP\pm}K^+)}{\Gamma(B^- \to D^0 K^-) + \Gamma(B^+ \to \bar{D}^0 K^+)}, \quad (2)$$

where $D_{CP\pm}$ refer to the *CP* eigenstates of the D meson system. We then extract γ, together with the other two unknowns r_B and δ_B, by means of a frequentist procedure, which exploits the following relations [4,5], neglecting D^0-$\bar{D}^0$ mixing [18]:

$$R_{CP\pm} = 1 + r_B^2 \pm 2r_B \cos\delta_B \cos\gamma, \quad (3)$$

$$A_{CP\pm} = \frac{\pm 2r_B \sin\delta_B \sin\gamma}{1 + r_B^2 \pm 2r_B \cos\delta_B \cos\gamma}. \quad (4)$$

Here, $r_B \equiv |A(B^- \to \bar{D}^0 K^-)/A(B^- \to D^0 K^-)|$ is the magnitude of the ratio of the amplitudes for $B^- \to \bar{D}^0 K^-$ and $B^- \to D^0 K^-$ and δ_B the difference of their strong phases. Taking into account the CKM factor ($|V_{ub}V_{cs}/V_{cb}V_{us}| \approx 0.4$) and color-suppression of the $B^- \to \bar{D}^0 K^-$ amplitude, r_B is expected to be around 0.1. The current world averages for the $B^\pm \to DK^\pm$ GLW observables from the measurements in [9,19,20] are summarized in Table I. The world averages for the parameters r_B and δ_B

TABLE I. World averages at 68% confidence level [21] for the GLW observables in $B \to DK$ decays.

CP of the D	R_{CP}	A_{CP}
+1	1.10 ± 0.09	0.24 ± 0.07
−1	1.06 ± 0.10	-0.10 ± 0.08

are $r_B = 0.104^{+0.015}_{-0.025}$ and $\delta_B = (117^{+17}_{-24})°$ at 68% confidence level (CL) [3].

To reduce the systematic uncertainties from branching fractions and reconstruction efficiencies of different D channels appearing in the numerator and denominator of Eq. (2), we approximate $R_{CP\pm}$ with the double ratios

$$R_{CP\pm} \approx \frac{R^\pm_{K/\pi}}{R_{K/\pi}}, \quad (5)$$

where

$$R^\pm_{K/\pi} \equiv \frac{\Gamma(B^- \to D_{CP\pm}K^-) + \Gamma(B^+ \to D_{CP\pm}K^+)}{\Gamma(B^- \to D_{CP\pm}\pi^-) + \Gamma(B^+ \to D_{CP\pm}\pi^+)}, \quad (6)$$

and

$$R_{K/\pi} \equiv \frac{\Gamma(B^- \to D^0 K^-) + \Gamma(B^+ \to \bar{D}^0 K^+)}{\Gamma(B^- \to D^0 \pi^-) + \Gamma(B^+ \to \bar{D}^0 \pi^+)}. \quad (7)$$

Equation (5) would be exact in the limit in which the Cabibbo-suppressed contributions to the $B^\pm \to D\pi^\pm$ amplitudes vanish, as well as terms proportional to $r_B r_D \approx 5 \times 10^{-3}$, as we will discuss in Sec. VII. This approximation results in a systematic uncertainty on the final values of $R_{CP\pm}$.

The paper is organized as follows. In Sec. III we describe the data sample used for these measurements and the main features of the *BABAR* detector and of the PEP-II storage rings. In Sec. IV we summarize the procedure adopted to select $B^\pm \to Dh^\pm$ candidates and suppress the main backgrounds. In Sec. V we introduce the simultaneous extended maximum likelihood fit used to extract the observables $R_{CP\pm}$ and $A_{CP\pm}$. In Sec. VI we explain how, by applying the same fit procedure to selected control samples, we estimate the irreducible background present in the final samples. A discussion of the sources of systematic uncertainties and the evaluation of the uncertainties is presented in Sec. VII. Section VIII lists the final results on the GLW observables $R_{CP\pm}$ and $A_{CP\pm}$, including statistical and systematic uncertainties. It also contains a description of the statistical method used to construct frequentist confidence intervals for the parameters γ, δ_B, and r_B. Section IX gives a summary of our results.

III. DATA SAMPLE AND DETECTOR

The measurements presented in this paper use the entire $B\bar{B}$ data sample collected with the *BABAR* detector at the PEP-II asymmetric-energy B factory at the SLAC National Accelerator Laboratory. The $B\bar{B}$ pairs are produced from the decays of $\Upsilon(4S)$ mesons that originate in collisions of 9.0 GeV electrons and 3.1 GeV positrons ($\sqrt{s} = 10.58$ GeV $= M_{\Upsilon(4S)}c^2$). In total, $(467 \pm 5) \times 10^6$ $B\bar{B}$ pairs, approximately equally divided into $B^0\bar{B}^0$ and B^+B^-, have been collected in the years from 1999 until early 2008. The B meson pairs are produced almost at rest in the $\Upsilon(4S)$ center-of-mass (CM) frame, but the

asymmetric beam energies boost them in the laboratory frame by $(\beta\gamma)_{CM} \approx 0.56$.

The *BABAR* detector is described in detail elsewhere [22]. Primary and secondary vertex reconstruction and charged-particle tracking are provided by a five-layer double-sided silicon vertex tracker and a 40-layer drift chamber. Charged particle identification (PID) is provided by measurement of specific ionization energy loss in the tracking devices and of the Cherenkov radiation cone in a ring-imaging detector. Photons and electrons are identified by combining the information from the tracking devices and the energy deposits in the electromagnetic calorimeter, which consists of 6580 thallium-doped CsI crystals. These systems are located inside a 1.5 T solenoidal superconducting magnet. Finally, the flux return of the magnet is instrumented with resistive plate chambers and limited streamer tubes in order to discriminate muons from pions. We use the GEANT4 [23] software toolkit to simulate interactions of particles in the detector, taking into account the varying accelerator and detector conditions.

IV. EVENT SELECTION

We reconstruct $B^{\pm} \to Dh^{\pm}$ decays, where the charged track h is either a kaon or a pion. Neutral D mesons are reconstructed in the *CP*-even eigenstates $\pi^{-}\pi^{+}$ and $K^{-}K^{+}$ (D_{CP+}), in the *CP*-odd eigenstates $K_S^0\pi^0$, $K_S^0\phi$ and $K_S^0\omega$ (D_{CP-}), and in the non-*CP*-eigenstate $K^{-}\pi^{+}$ (D^0 from $B^{-} \to D^0h^{-}$) or $K^{+}\pi^{-}$ ($\bar{D}^0$ from $B^{+} \to \bar{D}^0h^{+}$). *CP* violation in the K^0-$\bar{K}^0$ system is neglected, i.e. the K_S^0 is assumed to be a pure $CP = +1$ eigenstate. The D_{CP} daughters are reconstructed in the decay modes $K_S^0 \to \pi^{+}\pi^{-}$, $\phi \to K^{+}K^{-}$ and $\omega \to \pi^{-}\pi^{+}\pi^0$.

We optimize all our event selection requirements by maximizing the significance of the expected $B^{\pm} \to DK^{\pm}$ signal yield, defined as $N_{\text{sig}}/\sqrt{N_{\text{sig}} + N_{\text{bkg}}}$, where N_{sig} (N_{bkg}) is the expected signal (background) yield. The optimization is done for each D decay channel using simulated signal and background events, which are generated with the EVTGEN software package [24].

Neutral pions are reconstructed by combining pairs of photon candidates with energy deposits larger than 30 MeV that are not matched to charged tracks and whose energy deposition profile is consistent with that expected from a photon. The photon pair invariant mass is required to differ from the nominal π^0 mass [25] by less than 2.5 times its resolution ($\sigma \approx 6$ MeV/c^2) and the total π^0 energy in the laboratory frame must be greater than 240 MeV for $D \to K_S^0\pi^0$ and 210 MeV for $\omega \to \pi^{+}\pi^{-}\pi^0$.

Neutral kaons are reconstructed from pairs of oppositely charged tracks with invariant mass within 2.5σ ($\sigma \approx 2.1$ MeV/c^2) of the nominal K_S^0 mass [25]. The ratio between the K_S^0 signed 3-dimensional flight length and its uncertainty, determined from the position of the K_S^0 and the D decay vertices and the K_S^0 momentum direction, must be

greater than 1.9, 2.0, and 2.2 for $D \to K_S^0\pi^0$, $D \to K_S^0\phi$, and $D \to K_S^0\omega$, respectively.

The ϕ candidates are reconstructed from pairs of oppositely charged tracks passing kaon identification criteria with typical kaon selection efficiency of $\approx 98\%$ and pion misidentification of $\approx 15\%$. The two tracks are assigned the kaon mass hypothesis and their invariant mass is required to be within 6.5 MeV/c^2 of the nominal ϕ mass [25] (the resolution is $\sigma = 1.0$ MeV/c^2 and the natural width is $\Gamma_{\phi} = 4.3$ MeV). We also require that the helicity angle θ_H between the flight direction of one of the two kaons and the D flight direction, in the ϕ rest frame, satisfies the condition $|\cos\theta_H| > 0.4$. This requirement exploits the fact that in $D \to K_S^0\phi$ decays the ϕ is produced in a longitudinally polarized state, thus $\cos\theta_H$ follows a $\cos^2\theta_H$ distribution, while in ϕ candidates not from $D \to K_S^0\phi$ decays, $\cos\theta_H$ is approximately uniformly distributed.

The ω candidates are reconstructed from $\pi^{+}\pi^{-}\pi^0$ combinations with invariant mass within 17 MeV/c^2 ($2\Gamma_{\omega}$) of the nominal ω mass [25] (the resolution is $\sigma = 6.9$ MeV/c^2). The charged pion candidates are required to pass pion identification criteria with pion selection efficiency around 98% and kaon misidentification rate around 12%. To improve the ω momentum resolution, the invariant mass of the two photons forming the π^0 candidate is constrained to the nominal π^0 mass. We define θ_N as the angle between the normal to the ω decay plane and the D momentum in the ω rest frame, and $\theta_{\pi\pi}$ as the angle between the flight direction of one of the three pions in the ω rest frame and the flight direction of one of the other two pions in the two-pion rest frame. The quantities $\cos\theta_N$ and $\cos\theta_{\pi\pi}$ follow $\cos^2\theta_N$ and $(1 - \cos^2\theta_{\pi\pi})$ distributions, respectively, for the signal, and are almost uniformly distributed for wrongly reconstructed ω candidates. We require the product $\cos^2\theta_N\sin^2\theta_{\pi\pi} > 0.046$.

Neutral D candidates are formed from two-body combinations of $K^{\pm}$, $\pi^{\pm}$, K_S^0, π^0, ϕ and ω candidates consistent with one of the six D decay channels under study. To improve the D_{CP-} momentum resolution, the invariant masses of the π^0 and K_S^0 daughters are constrained to the nominal π^0 and K_S^0 masses. To suppress poorly reconstructed D candidates and candidates from random combinations, we perform a geometric fit of the D daughters to a common origin, and reject D candidates for which the χ^2 probability of the vertex fit is lower than 0.01%. The invariant mass of a D candidate M_D must be within a range that corresponds to slightly more than twice the M_D resolution: the range varies from about ± 6 MeV/c^2 for the $K_S^0\phi$ channel to about ± 44 MeV/c^2 for the $K_S^0\pi^0$ channel. We apply the following particle identification criteria to the charged daughters of the D meson: in $D \to \pi^{+}\pi^{-}$, the two-pion candidates must pass the same pion identification criteria adopted in the reconstruction of $\omega \to \pi^{-}\pi^{+}\pi^0$; in $D \to K^{+}K^{-}$, the two kaon candidates are required to pass

tighter kaon identification criteria than those applied to the ϕ daughters (typical kaon selection efficiency around 94%, and pion misidentification rate around 6%); in $D \rightarrow K^- \pi^+$, the kaon candidate must pass the same kaon identification criteria required for the ϕ daughters. In order to reduce the large combinatorial background from random combinations of tracks and photons in $e^+ e^- \rightarrow q\bar{q}$ events ($q = u, d, s, c$), we put requirements on the cosine of the D decay angle, $|\cos\theta_D|$. We define θ_D as the angle between one of the D daughters in the D rest frame, and the direction of the D meson in the B rest frame. Because of angular momentum conservation we expect the distribution of $\cos\theta_D$ to be uniform for $B^\pm \rightarrow Dh^\pm$, $D \rightarrow \pi^+ \pi^-$ and $D \rightarrow K_S^0 \pi^0$ signal events, while for $q\bar{q}$ events the distribution is strongly peaked at ± 1. We require $|\cos\theta_D| < 0.74$ (0.99) for the $B^\pm \rightarrow Dh^\pm$, $D \rightarrow \pi^+ \pi^-$ ($D \rightarrow K_S^0 \pi^0$) channel.

The invariant mass distributions of the reconstructed D candidates, after all the other selection criteria described in this section have been applied, are shown in Fig. 1.

We reconstruct $B^\pm$ meson candidates by combining a neutral D candidate with a track $h^\pm$. For the $D \rightarrow K\pi$ mode, the charge of the track h must match that of the kaon from the D meson decay. This selects $b \rightarrow c$ mediated B decays $B^- \rightarrow D^0 h^-$ and $B^+ \rightarrow \bar{D}^0 h^+$. The contamination from $b \rightarrow u$ mediated B decays followed by doubly-Cabibbo-suppressed D decay, i.e. $B^- \rightarrow \bar{D}^0 K^-$, $\bar{D}^0 \rightarrow K^- \pi^+$, and from D^0-$\bar{D}^0$ mixing is negligible. In the $B^\pm \rightarrow Dh^\pm$, $D \rightarrow \pi^+ \pi^-$ channel we require that the invariant mass of the $(h^\pm \pi^\mp)$ system is greater than 1.9 GeV/c^2 to reject background from $B^- \rightarrow D^0 \pi^-$, $D^0 \rightarrow K^- \pi^+$ and $B^- \rightarrow K^{*0} \pi^-$, $K^{*0} \rightarrow K^- \pi^+$ decays and their CP conjugates. Here π is the pion from the D and h is the track from the B candidate taken with the kaon mass hypothesis. To improve the B momentum resolution, the neutral D invariant mass is constrained to the nominal D^0 mass [25] for all D decay channels.

We identify signal $B \rightarrow DK$ and $B \rightarrow D\pi$ candidates using two kinematic variables: the difference between the CM energy of the B meson (E_B^*) and the beam energy,
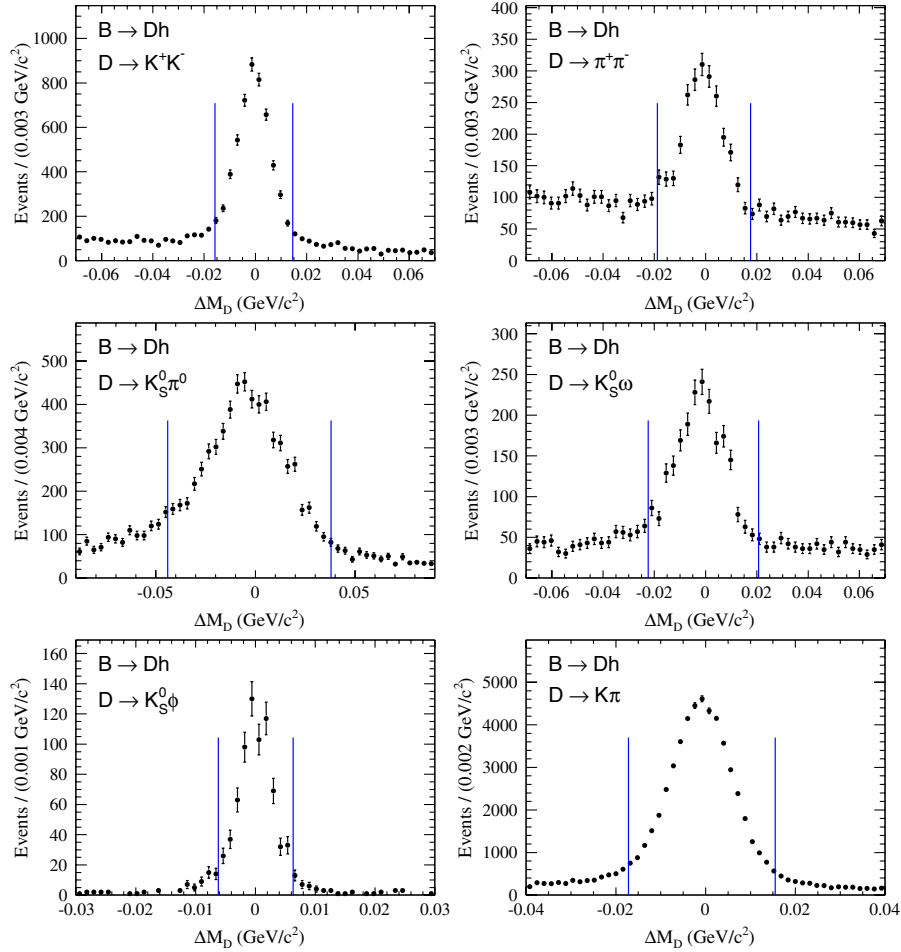
FIG. 1 (color online). Distributions of the difference between the D candidate's invariant mass and the nominal D^0 mass [25], as measured in the $B^\pm \rightarrow Dh^\pm$ samples. All selection criteria described in Sec. IV, except that on the D invariant mass M_D, have been applied, including the χ^2-based candidate selection. In addition we reduce the background by requiring the fit variables to satisfy $m_{\text{ES}} > 5.27$ GeV/c^2, $\Delta E > -0.05$ GeV, and $\mathcal{F} > -0.25$. The ΔM_D selection requirements are depicted by the vertical lines.

$$\Delta E = E_B^* - \sqrt{s}/2, \qquad (8)$$

and the beam-energy-substituted mass,

$$m_{\text{ES}} = \sqrt{(s/2 + \mathbf{p}_{ee} \cdot \mathbf{p}_B)^2/E_{ee}^2 - p_B^2}, \qquad (9)$$

where $(E_B, \mathbf{p}_B)$ and $(E_{ee}, \mathbf{p}_{ee})$ are the four-momenta of the B meson and of the initial e^+e^- system, respectively, measured in the laboratory frame. The m_{ES} distributions for $B^\pm \rightarrow Dh^\pm$ signals are centered at the B mass [25], have a root-mean-square of approximately 2.6 MeV/c^2, and do not depend strongly on either the D decay mode or the nature of the track h. In contrast, the ΔE distributions depend on the mass assigned to the track h. We evaluate ΔE with the kaon mass hypothesis so that the peaks of the distributions are centered near zero for $B^\pm \rightarrow DK^\pm$ events and are shifted by approximately $+50$ MeV for $B^\pm \rightarrow D\pi^\pm$ events. The ΔE resolution depends on the kinematics of the decay, and is typically 16 MeV for all D decay modes under study after the D invariant mass is constrained to its nominal value. We retain B candidates with m_{ES} and ΔE within the intervals $5.20 < m_{\text{ES}} < 5.29$ GeV/c^2 and $-80 < \Delta E < 120$ MeV, which define the region for the fit described later.

In order to discriminate the signal from $e^+e^- \rightarrow q\bar{q}$ background events, denoted $q\bar{q}$ in the following, we construct a Fisher discriminant $\mathcal{F}$ based on the four event-shape quantities L_{20}^{ROE}, $|\cos\theta_T^*|$, $|\cos\theta_B^*|$ and H_{20}^{ROE}. These quantities, evaluated in the CM frame, are defined as

(i) $L_{20}^{\text{ROE}} = L_2/L_0$ is the ratio of the second and zeroth event shape moments of the energy flow in the rest of event (ROE), i.e. considering all the charged tracks and neutral clusters in the event that are not used to reconstruct the B candidate. They are defined as $L_2 = \sum_i p_i \cos^2\theta_i$ and $L_0 = \sum_i p_i$, where p_i are the momenta and θ_i the angles of the charged and neutral particles in the ROE, with respect to the thrust axis of the B candidate's decay products. The thrust axis is defined as the direction that maximizes the sum of the longitudinal momenta of the particles used to define it;

(ii) θ_T^* is the angle between the thrust axis of the B candidate's decay products and the beam axis;

(iii) θ_B^* is the angle between the B candidate momentum and the beam axis;

(iv) $H_{20}^{\text{ROE}} = H_2/H_0$ is the ratio of the second and zeroth Fox-Wolfram moments H_2 and H_0 [26], computed using charged tracks and photons in the ROE.

The quantity $\mathcal{F}$ is a linear combination of the four aforementioned event-shape variables:

$$\mathcal{F} = c_1 L_{20}^{\text{ROE}} + c_2|\cos\theta_T^*| + c_3|\cos\theta_B^*| + c_4 H_{20}^{\text{ROE}}. \qquad (10)$$

The values of the coefficients c_i are the ones which maximize the separation between simulated signal events and a continuum background sample provided by off-resonance data, taken ≈ 40 MeV below the $\Upsilon(4S)$ resonance. The maximum likelihood fit described in Sec. V is restricted to events with $\mathcal{F}$ within the interval $-1.5 < \mathcal{F} < 1.5$, to remove poorly reconstructed candidates.

For events with multiple $B^\pm \rightarrow Dh^\pm$ candidates (about 16% of the selected events), we choose the B candidate with the smallest $\chi^2 = \sum_c (M_c - M_c^{\text{PDG}})^2/(\sigma_{M_c}^2 + \Gamma_c^2)$ formed from the measured and true masses, M_c and M_c^{PDG}, of all the unstable particles c produced in the B decay tree (D, π^0, K_S^0, ϕ, ω), scaled by the sum in quadrature of the resolution σ_{M_c} of the reconstructed mass and the intrinsic width Γ_c. From simulated signal events, we find that this algorithm has a probability to select the correct candidate between 98.2% and 99.9% depending on the D decay mode. We also find that the algorithm has negligible effect on the M_D distributions.

We compare the distribution of each selection variable in data and simulated events after the requirements on all other variables have been applied. In order not to introduce biases that may artificially enhance the signal yield, we perform a blind study by explicitly removing, in this comparison, events consistent with the $B^\pm \rightarrow DK^\pm$ signal, i.e. those with $|m_{\text{ES}} - m_B| < 10$ MeV/c^2, $|\Delta E| < 40$ MeV, $\mathcal{F} > -0.8$ and track h passing kaon identification criteria. We find excellent agreement between data and simulated events, both for events consistent with the $B^\pm \rightarrow D\pi^\pm$ signal ($|m_{\text{ES}} - m_B| < 10$ MeV/c^2, $|\Delta E - 50$ MeV$| < 40$ MeV, $\mathcal{F} > -0.8$ and track h failing the kaon identification criteria) and for backgroundlike events. We correct for small differences in the means and widths of the distributions of the invariant masses of the unstable particles and of m_{ES} and ΔE both when applying to data the selection criteria obtained from simulated events and in the final fit described in the next section.

The total reconstruction efficiencies, based on simulated $B^\pm \rightarrow DK^\pm$ events, are summarized in the second column of Table II. For the reasons explained in Sec. II, the efficiencies are 40% to 60% higher than in our previous study of the same decay channels [9]. The efficiencies obtained for $B^\pm \rightarrow D\pi^\pm$ events from the simulation are

TABLE II. Reconstruction efficiency for $B \rightarrow DK$ from simulated events. We also quote the efficiency and purity in a signal-enriched subsample (see text for details).

D^0 mode	Efficiency after full selection	Efficiency in signal-enriched subsample	Purity in signal-enriched subsample
$K^-\pi^+$	52%	22%	96%
K^+K^-	44%	18%	85%
$\pi^+\pi^-$	38%	17%	68%
$K_S^0\pi^0$	24%	10%	83%
$K_S^0\phi$	20%	9%	91%
$K_S^0\omega$	10%	4%	71%

statistically consistent with those for $B^\pm \to DK^\pm$, where the D meson is reconstructed in the same final state. For illustration purposes we define a signal-enriched sample for each D decay mode, containing all $B^\pm \to Dh^\pm$ candidates satisfying the criteria $-40 < \Delta E < 100$ MeV, $0.2 < \mathcal{F} < 1.5$, $5.275 < m_{\mathrm{ES}} < 5.285$ GeV/c^2, and whose daughter track h passes charged kaon identification criteria. The typical kaon efficiency is $\approx 77\%$ and the pion misidentification rate is $\approx 2\%$. The reconstruction efficiencies and the expected purities for the signal-enriched subsamples, determined on simulated data, are listed in Table II.

V. MAXIMUM LIKELIHOOD FIT

We measure $R_{K/\pi}^{(\pm)}$ and $A_{CP\pm}$ using simultaneous extended and unbinned maximum likelihood fits to the distributions of the three variables ΔE, m_{ES}, and $\mathcal{F}$ of B candidates selected in data. The data set is split into 24 subgroups by means of three discrete variables: the charge $\eta = \pm 1$ of the reconstructed B meson ($\times 2$ subgroups); the two-body D decay final state X ($\times 6$), allowing for a more accurate description of the corresponding probability density functions compared to the larger $CP\pm$ subgroups; and a PID variable denoting whether or not the track h from the B passes (p) or fails (f) charged kaon identification criteria ($\times 2$). The pion misidentification rate of these criteria is determined directly from data as described later, and is expected from simulation to be around 2%. The corresponding kaon identification efficiency is $(77 \pm 1)\%$, as determined from the signal MC samples after weighting the bidimensional distribution of the momentum and polar angle of the track h by the ratio of the analogous distributions observed in MC and data kaon control samples. The uncertainty on the kaon identification efficiency is dominated by the systematic contribution from the uncertainties on the weights. We perform in total three simultaneous fits to these 24 subgroups: one fit for the two CP-even D final states (8 subgroups), one for the three CP-odd D final states (12 subgroups), and one for the $D \to K\pi$ decay (4 subgroups).

The likelihood function $\mathcal{L}$ for each of these simultaneous fits has the form

$$\mathcal{L}(\vec{\nu}) = \frac{e^{-N} N^n}{n!} \prod_s \prod_{i=1}^{N_s} \mathcal{P}_s(m_{\mathrm{ES},i}, \Delta E_i, \mathcal{F}_i; \vec{\nu}), \quad (11)$$

where s ranges over the subgroups under consideration, N_s is the number of events in subgroup s, n is the total number of events in the fit $n = \sum_s N_s$, and N is the expected number of events. We minimize $-\ln \mathcal{L}$ with respect to the set of fit parameters $\vec{\nu}$ specified later. The probability $\mathcal{P}_{s,i} \equiv \mathcal{P}_s(m_{\mathrm{ES}i}, \Delta E_i, \mathcal{F}_i)$ for an event i is the sum of six signal and background components: $B^\pm \to DK^\pm$ signal, $B^\pm \to D\pi^\pm$ signal, background candidates from $e^+ e^- \to q\bar{q}$

events, irreducible background arising from charmless $B^\pm \to XK^\pm$ and $B^\pm \to X\pi^\pm$ decays, and background candidates from other $B\bar{B}$ events (reducible $B\bar{B}$ background):

$$N_s \mathcal{P}_{s,i} = N_s^{D\pi} \mathcal{P}_{s,i}^{D\pi} + N_s^{DK} \mathcal{P}_{s,i}^{DK} + N_s^{q\bar{q}} \mathcal{P}_{s,i}^{q\bar{q}} + N_s^{B\bar{B}} \mathcal{P}_{s,i}^{B\bar{B}} \\ + N_s^{X\pi} \mathcal{P}_{s,i}^{X\pi} + N_s^{XK} \mathcal{P}_{s,i}^{XK}, \quad (12)$$

where the N_s^j are the expected yields in each component j. In case of negligible correlations among the fit variables, each probability density function (PDF) $\mathcal{P}$ factorizes as

$$\mathcal{P}(m_{\mathrm{ES}}, \Delta E, \mathcal{F}) = \mathcal{P}(m_{\mathrm{ES}}) \mathcal{P}(\Delta E) \mathcal{P}(\mathcal{F}). \quad (13)$$

The irreducible $B\bar{B}$ background originates from events where a B meson decays to the same final state Xh as the signal, but without the production of an intermediate charmed meson in the decay chain. When exploiting the ΔE, m_{ES}, and $\mathcal{F}$ variables, this background is therefore indistinguishable from the signal. As an example, the decay $B^\pm \to K^+ K^- K^\pm$ ($X = K^+ K^-$) is an irreducible background for $B^\pm \to D_{CP+} K^\pm$, $D_{CP+} \to K^+ K^-$. As described later in Sec. VI, the irreducible background yield can be estimated by studying sideband regions of the D candidate invariant mass distribution, and can then be fixed in the final fit, where we assume $\mathcal{P}_i^{Dh} = \mathcal{P}_i^{Xh}$.

We express the signal yield parameters N_s^{DK} and $N_s^{D\pi}$ through the CP asymmetries A_{DK}^X and $A_{D\pi}^X$ of $B^\pm \to DK^\pm$, $D \to X$ and $B^\pm \to D\pi^\pm$, $D \to X$, their branching fraction ratios, $R_{K/\pi}^X$, the total number $N_{\mathrm{tot},X}^{D\pi}$ of $B^\pm \to D\pi^\pm$, $D \to X$ signal events, the true kaon identification efficiency ε of the PID selector, and the pion misidentification rate m of the PID selector:

$$N_{\eta,p,X}^{DK} = \frac{1}{2}(1 - \eta A_{DK}^X) N_{\mathrm{tot},X}^{D\pi} R_{K/\pi}^X \varepsilon, \quad (14)$$

$$N_{\eta,f,X}^{DK} = \frac{1}{2}(1 - \eta A_{DK}^X) N_{\mathrm{tot},X}^{D\pi} R_{K/\pi}^X (1 - \varepsilon), \quad (15)$$

$$N_{\eta,p,X}^{D\pi} = \frac{1}{2}(1 - \eta A_{D\pi}^X) N_{\mathrm{tot},X}^{D\pi} m, \quad (16)$$

$$N_{\eta,f,X}^{D\pi} = \frac{1}{2}(1 - \eta A_{D\pi}^X) N_{\mathrm{tot},X}^{D\pi} (1 - m). \quad (17)$$

Because the ratios $R_{K/\pi}^X$ are small, the fit is not able to determine the value of ε. Therefore we fix it to the aforementioned value of $\varepsilon = (77 \pm 1)\%$. The reconstruction and selection efficiencies for true $B^\pm \to DK^\pm$ and $B^\pm \to D\pi^\pm$ candidates, where the D meson decays to the same final state, are assumed to be identical. A systematic uncertainty is assigned due to this assumption (see Sec. VII). The simultaneous fit to the two CP-even modes constrains

$$A_{DK}^{\pi^+ \pi^-} = A_{DK}^{K^+ K^-} \equiv A_{CP+}, \quad (18)$$

$$R_{K/\pi}^{\pi^+\pi^-} = R_{K/\pi}^{K^+K^-} \equiv R_{K/\pi}^+, \qquad (19)$$

while the simultaneous fit to the three *CP*-odd modes constrains

$$A_{DK}^{K_S^0\pi^0} = A_{DK}^{K_S^0\phi} = A_{DK}^{K_S^0\omega} \equiv A_{CP-}, \qquad (20)$$

$$R_{K/\pi}^{K_S^0\pi^0} = R_{K/\pi}^{K_S^0\phi} = R_{K/\pi}^{K_S^0\omega} \equiv R_{K/\pi}^-. \qquad (21)$$

The m_{ES} distributions of the signal components are parametrized using an asymmetric Gaussian shape, i.e. a Gaussian with different widths on both sides of the peak. We use the same shape for $B^\pm \to DK^\pm$ and $B^\pm \to D\pi^\pm$, so the m_{ES} $B^\pm \to DK^\pm$ signal shape (whose parameters are floating in the fit) will mostly be determined by the much more abundant $B^\pm \to D\pi^\pm$ control sample. Since the selection efficiencies for the two channels are the same, we expect the number of reconstructed candidates from $B^\pm \to D\pi^\pm$ to be about 12 times higher than for $B^\pm \to DK^\pm$. We have checked that the m_{ES} shapes for $B^\pm \to DK^\pm$ and $B^\pm \to D\pi^\pm$ are consistent, and that the assumption that they are identical does not bias the parameters of interest.

The ΔE distribution of the $B^\pm \to DK^\pm$ signal component is parametrized with a double Gaussian shape. The core Gaussian has a mean close to zero, a width around 16 MeV and, according to the simulation, accounts for about 90% of the true $B^\pm \to DK^\pm$ candidates. The second Gaussian accounts for the remaining 10% of candidates whose energy has been poorly measured. The mean and width of the core Gaussian are directly determined from data, while the remaining three parameters (the difference between the two means, the ratio between the two widths and the ratio of the integrals of the two Gaussian functions) are fixed from the simulation. In contrast to the m_{ES} case, the $B^\pm \to D\pi^\pm$ ΔE shape is not the same as for $B^\pm \to DK^\pm$. This is due to the fact that we always assign the kaon mass hypothesis to the track h: the wrong mass assignment, in the case of $B^\pm \to D\pi^\pm$, introduces a shift to the reconstructed energy of the pion and thus to ΔE, since $\Delta E = E_B^* - \sqrt{s}/2 = E_D^* + E_h^* - \sqrt{s}/2$. The shift depends on the magnitude of the momentum **p** of the track h in the laboratory frame,

$$\Delta E_{\text{shift}}(\mathbf{p}) = \gamma_{CM}(\sqrt{m_K^2 + \mathbf{p}^2} - \sqrt{m_\pi^2 + \mathbf{p}^2}). \qquad (22)$$

Therefore we parametrized the $B^\pm \to D\pi^\pm$ ΔE signal component with the sum of two Gaussians whose means are computed event-per-event by adding $\Delta E_{\text{shift}}(\mathbf{p})$ to the means of the Gaussian functions used to describe the $B^\pm \to DK^\pm$ ΔE signal. The other parameters of the $B^\pm \to D\pi^\pm$ and $B^\pm \to DK^\pm$ ΔE distributions (the two widths and the ratio of the integrals) are identical. Again, we exploit the $B^\pm \to D\pi^\pm$ control sample to determine the shape of the $B^\pm \to DK^\pm$ signal. In the case of the high statistics flavor mode $D \to K\pi$, we add a linear back-

ground component to the double Gaussian shape to account for misreconstructed events, which peak in m_{ES} but not in ΔE. The ratio between the integral of the linear component and that of the two Gaussian functions is fixed from simulated signal events.

For the reducible $B\bar{B}$ background, Eq. (13) does not hold because of significant correlations between the ΔE and m_{ES} distributions. This reflects the fact that this background is composed of two categories of B candidates with different m_{ES} and ΔE distribution:

(i) B candidates formed from random combinations of charged tracks and neutral objects in the event, which populate the whole m_{ES}-ΔE plane;

(ii) B candidates from $B^\pm \to D\rho^\pm$, $B^\pm \to DK^{*\pm}$, $B^\pm \to D^*h^\pm$ ($D^* \to D\pi$), where a pion from the ρ, K^* or D^* decay is not reconstructed. These candidates peak in m_{ES} close to the B mass, but with broader resolution compared to the signal, and are shifted towards negative ΔE values, typically peaking at $\Delta E \approx -m_\pi c^2$, therefore outside of the ΔE fit region; however, the tail on the positive side of the distribution extends into the ΔE fit region.

We parametrize the m_{ES}-ΔE distribution of the $B\bar{B}$ background by means of two factorizing components:

$$\mathcal{P}_{B\bar{B}}(m_{ES}, \Delta E) = f \times g_{\text{peak}}(m_{ES})h_{\text{peak}}(\Delta E) + (1 - f)$$
$$\times g_{\text{cont}}(m_{ES})h_{\text{cont}}(\Delta E). \qquad (23)$$

The m_{ES} component of the peaking part, $g_{\text{peak}}(m_{ES})$, is parametrized with a Gaussian function for $X = \pi^+\pi^-$, $K_S^0\omega$, $K_S^0\phi$. For $X = K^+K^-$, $K_S^0\pi^0$ we use the "Crystal Ball" lineshape [27], an empirical smooth function that better describes the non-Gaussian tail on the negative side of the distribution,

$$C(x) = \begin{cases} \frac{n^n}{|\alpha|^n} e^{-(|\alpha|^2/2)} \left(\frac{n}{|\alpha|} - |\alpha| - \bar{x} \right)^{-n} & \bar{x} < -|\alpha|, \\ \exp\left(-\frac{1}{2}\bar{x}^2\right) & \bar{x} \geq -|\alpha|, \end{cases}$$
$$\qquad (24)$$

with $\bar{x} = (x - \mu)/\sigma$ and $\bar{x} \to -\bar{x}$ for $\alpha < 0$. For $X = K\pi$ we use an empirical function of the form:

$$N(x) = \exp\left(-\frac{1}{2\tau^2}\{\ln^2[1 + \Lambda\tau(x - \mu)] + \tau^4\}\right), \qquad (25)$$

with $\Lambda = \sinh(\tau\sqrt{\ln 4})/(\sigma\tau\sqrt{\ln 4})$. Here μ is the position of the peak, while σ and τ are parameters related to the width of the distribution on the two sides of the peak. The ΔE component of the peaking part $h_{\text{peak}}(\Delta E)$ is described with a simple exponential function for the five *CP* self-conjugate D final states, and with a Landau function for the non-*CP*-eigenstate final state. The $B\bar{B}$ purely combinatorial background component is described by the 2-dimensional product of a linear background, $h_{\text{cont}}(\Delta E)$, and an empirical function introduced by the ARGUS Collaboration [28], $g_{\text{cont}}(m_{ES}) = A(m_{ES}/m_0)$:

$$A(x) = x(1 - x^2)^p \exp(-\zeta[1 - x^2]), \qquad (26)$$

where $m_0 = \sqrt{s}/(2c^2) = 5.29 \text{ GeV}/c^2$ is the kinematic endpoint of the m_{ES} distribution. All the parameters of the $B\bar{B}$ background m_{ES}-ΔE distribution are fixed from simulated $B\bar{B}$ events. The only exception is the width of the Landau function used for $h_{\mathrm{peak}}(\Delta E)$ in $X = K^-\pi^+$. This parameter controls the behavior at low ΔE values, $\Delta E \approx -80 \text{ MeV}$, where we find the simulation not to be sufficiently precise given the high statistics of this channel. We note that the shape parameters differ across the six final states, but are similar across the charge and PID selector subgroups belonging to one final state.

In $q\bar{q}$ events, B candidates arise from random combinations of charged tracks and neutral particles produced in the hadronization of the light quark-antiquark pairs produced in e^+e^- collisions. Similarly to the combinatorial component of the $B\bar{B}$ background, the $q\bar{q}$ background distribution in the m_{ES}-ΔE plane is parameterized by the product of an ARGUS function in m_{ES} and a linear background in ΔE. We float the slope of the linear components, while the parameters of the ARGUS function are fixed, in each D final state, from simulated $q\bar{q}$ events. They are in good agreement across the final states and other subgroups.

The $\mathcal{F}$ distributions are parametrized in a similar way for all fit components. We find that the distributions of $B^\pm \rightarrow DK^\pm$ and $B^\pm \rightarrow D\pi^\pm$ signal events are consistent with each other, as expected since their kinematics are very similar, and choose to parametrize them with the same shape. For this we use the sum of two asymmetric Gaussian functions. Some channels with lower statistics do not require the full complexity of this parametrization: in those cases we use a single asymmetric Gaussian, a double Gaussian, or a single Gaussian. In particular we use: for the signal components a double asymmetric Gaussian, except for $X = K_S^0\phi$, where a double Gaussian function is adopted; for the $B\bar{B}$ background components a double asymmetric Gaussian in case of $X = K_S^0\pi^0, K^-\pi^+$, a double Gaussian in case of $X = K_S^0\omega$, and a single Gaussian otherwise; for the $q\bar{q}$ background components a double asymmetric Gaussian, except for $X = K_S^0\phi$, where we use a single Gaussian.

In summary, the floating parameters of the fits are all parameters related to the signal yields, and therefore to the GLW parameters, as given in Eqs. (14)–(17), except ε; all background yields and *CP*-asymmetries except the irreducible background yields and asymmetries, the $B\bar{B}$ asymmetries for *CP*− modes and for the $(CP+, p)$ subgroups ($B \rightarrow D_{CP+}h$ candidates where the track h passes the kaon identification criteria), and the $B\bar{B}$ yield in the $(K_S^0\phi, p)$ subgroup; selected shape parameters, namely, the overall width and mean of the ΔE signal, the m_{ES} signal shape, and the ΔE and $\mathcal{F}$ shape for $q\bar{q}$ background. The nonfloating parameters are fixed to their expectations obtained from simulation or, in case of the irreducible background yields, to values obtained from data control samples (see next section). Nonfloating *CP* asymmetries are fixed to zero. We assign systematic uncertainties due to the fixed parameters.

We check that the fitter is correctly implemented by generating and fitting a large number of test data sets using the final PDFs. In this study, we include an analytic description for the conditional variable $\Delta E_{\mathrm{shift}}$. The residuals for a given parameter, divided by the measured parameter error, should follow a Gaussian distribution with zero mean (μ) and unitary width (σ). We observe no significant deviations from the expected distribution. In particular, $R_{K/\pi}^+$ shows the largest shift from zero mean ($\mu = -0.06 \pm 0.07$) and A_{CP+} shows the largest deviation from unity width ($\sigma = 1.13 \pm 0.06$) among the parameters of interest.

We investigate fit biases, arising from possible discrepancies between the true signal distribution and the chosen fit model, by fitting a large number of test data sets, in which the $B^\pm \rightarrow DK^\pm$ and $B^\pm \rightarrow D\pi^\pm$ signal components are taken from simulated samples of sufficient statistics, while the background components are randomly generated according to their PDFs. Of all floating parameters, only $R_{K/\pi}$ acquires a significant bias, resulting in corrections of 0.5 and 1.0 times the expected statistical uncertainties on these parameters in the *CP* and flavor modes, respectively. This bias is caused by small differences in the ΔE distributions of the signal components across the kaon PID subgroups (p and f), which the final PDF does not account for. A second, smaller contribution to this bias is a small discrepancy between the $\Delta E(\pi)$ signal shape of $B^\pm \rightarrow D\pi^\pm$ events and the $\Delta E(K)$ shape of $B^\pm \rightarrow DK^\pm$ events. The biases in the $R_{K/\pi}$ parameters are correlated, and partly cancel in the ratio, resulting in a smaller bias on the GLW parameters $R_{CP\pm}$. The largest (smallest) remaining bias is 0.12 (0.05) times the expected statistical uncertainty for R_{CP+} (A_{CP-}). We correct the final values of the parameters A_{CP} and $R_{K/\pi}$ for the observed biases, and assign systematic uncertainties to these corrections.

VI. IRREDUCIBLE BACKGROUND DETERMINATION

As discussed in the previous section, the irreducible background arises from charmless $B^\pm \rightarrow Xh^\pm$ decays, which have the same final states as the $B^\pm \rightarrow D(\rightarrow X)h^\pm$ signal and therefore the same distribution of the three fit variables ΔE, m_{ES}, and $\mathcal{F}$.

In the $D^0 \rightarrow K^-\pi^+$ flavor mode, the irreducible background—taking into account the measured branching fractions for $B^\pm \rightarrow K^\pm\pi^\mp K^\pm$ and $B^\pm \rightarrow K^\pm\pi^\mp\pi^\pm$ [25] and a selection efficiency of $\approx 1\%$, estimated from simulated events—is negligible compared to the expected signal yields (about 3400 $B^\pm \rightarrow DK^\pm$ and 45000 $B^\pm \rightarrow D\pi^\pm$ expected signal events). On the other hand, in the *CP* modes, where the signal yields are expected to be an order of magnitude lower than in $K^-\pi^+$, and the upper limits for

the branching ratios of $B^\pm \to Xh^\pm$ decays are at the 10^{-5} level, we cannot *a priori* exclude a relevant irreducible background contribution.

We estimate the irreducible background yields in our sample by exploiting the fact that the D invariant mass distribution for this background is approximately uniform, while for the signal it is peaked around the nominal D mass. Therefore we can select a control sample containing irreducible background candidates, but with the signal strongly suppressed, by applying the same selection as for the signal, with the only difference that the D invariant mass is required to lie in a region (D invariant mass sidebands) which is separated by at least a few σ_{M_D} from the nominal D mass (see Table III). We then perform an extended maximum likelihood fit to the $m_{\rm ES}$, ΔE, and $\mathcal{F}$ distributions of the control sample in order to measure the irreducible background yields in the D invariant mass sidebands. The fit is similar to the nominal one described in the previous section. However, due to the limited statistics available in the sidebands, we are forced to fix more parameters compared to the nominal fit; in particular, we fix any possible charge asymmetry of the $B^\pm \to Xh^\pm$ decays to zero (a systematic uncertainty is assigned to this assumption). Finally, since the D candidate invariant mass distribution of the irreducible background is approximately uniform, we scale the obtained yields by the ratio of the widths of the D signal and control sideband mass regions to obtain the irreducible background yield N^{Xh} (scale factor in Table III). Table IV shows the scaled irreducible background yields that enter the final fit.

TABLE III. D mass sideband definitions, the scale factor defined as the ratio of the widths of the D mass signal and sideband regions.

D decay mode	M_D sideband region (MeV/c^2)	Scale factor
K^+K^-	$[1794.5 - 1834.5]$, $[1884.5 - 1914.5]$	0.43
$\pi^+\pi^-$	$[1814.5 - 1839.5]$, $[1889.5 - 1934.5]$	0.48
$K^0_S\pi^0$	$[1774.5 - 1804.5]$, $[1924.5 - 1954.5]$	1.67
$K^0_S\omega$	$[1794.5 - 1829.5]$, $[1899.5 - 1934.5]$	0.69
$K^0_S\phi$	$[1794.5 - 1834.5]$, $[1894.5 - 1934.5]$	0.28

TABLE IV. Irreducible background yields estimated from M_D sidebands in data.

D decay mode	N^{XK}	$N^{X\pi}$
K^+K^-	93 ± 10	-5 ± 8
$\pi^+\pi^-$	4 ± 6	0 ± 9
$K^0_S\pi^0$	-4 ± 9	65 ± 23
$K^0_S\omega$	3 ± 6	0 ± 8
$K^0_S\phi$	0.5 ± 0.7	1.4 ± 1.0

VII. SYSTEMATIC UNCERTAINTIES

We consider nine sources of systematic uncertainty that may affect the GLW parameters $A_{CP\pm}$ and $R_{CP\pm}$. Their contributions are summarized in Table V.

First, we estimate the influence of fixed parameters of the nominal PDF. We perform a large number of test fits to the data, similar to the nominal fit. In each of these test fits the fixed parameters are varied according to their covariance matrices. From the resulting distributions we calculate the systematic covariances of the fit parameters $A_{CP\pm}$ and $R_{K/\pi}$. The parameters responsible for the largest uncertainty are the $m_{\rm ES}$ endpoint m_0, and parameters related to the measured yields, e.g. $B\bar{B}$ background asymmetries and the efficiency of the kaon selector.

The uncertainties in the irreducible background event yields introduce a systematic uncertainty in the $B^\pm \to D_{CP}h^\pm$ yields and therefore in $R_{CP\pm}$. Likewise, any charge asymmetry in this background would affect the measured values of $A_{CP\pm}$. We again perform a series of test fits to on-peak data, where we vary the $B^\pm \to Xh^\pm$ yields and asymmetries by their uncertainties. For the latter, we take the uncertainties to be $\pm 10\%$ for $X = K^+K^-$ and $\pm 20\%$ for the other modes, which are conservative estimates consistent with the existing upper limits on the CP asymmetries in those decays [21].

As explained in Sec. V, we correct the fit results for biases observed in Monte Carlo studies. We take the

TABLE V. Summary of systematic uncertainties.

Source	A_{CP+}	A_{CP-}	R_{CP+}	R_{CP-}
Fixed fit parameters	0.004	0.005	0.026	0.022
Peaking background	0.014	0.005	0.017	0.013
Bias correction	0.004	0.004	0.006	0.005
Detector charge asym.	0.014	0.014	$\cdots$	$\cdots$
Opposite-CP background	$\cdots$	0.003	$\cdots$	0.006
$R_{CP\pm}$ vs $R_\pm$	$\cdots$	$\cdots$	0.026	0.023
Signal self cross-feed	0.0002	0.001	$\cdots$	$\cdots$
$\varepsilon(\pi)/\varepsilon(K)$	$\cdots$	$\cdots$	0.009	0.008
$\Delta E_{\rm shift}$ PDFs	0.007	0.011	0.029	0.024
Total	0.022	0.020	0.051	0.043

TABLE VI. Measured signal yields calculated from the fit results given in Table VIII using $N(B \to DK) = N^{\rm sig(\pi)}_{\rm tot} R_{K/\pi}$, $N(B \to D\pi) \equiv N^{\rm sig(\pi)}_{\rm tot}$, and error propagation neglecting small correlations.

D^0 mode	$N(B^\pm \to DK^\pm)$	$N(B^\pm \to D\pi^\pm)$
K^+K^-	367 ± 27	4091 ± 70
$\pi^+\pi^-$	110 ± 9	1230 ± 41
$K^0_S\pi^0$	338 ± 24	4182 ± 73
$K^0_S\omega$	116 ± 9	1440 ± 45
$K^0_S\phi$	52 ± 4	648 ± 27
$K^-\pi^+$	3361 ± 82	44631 ± 232
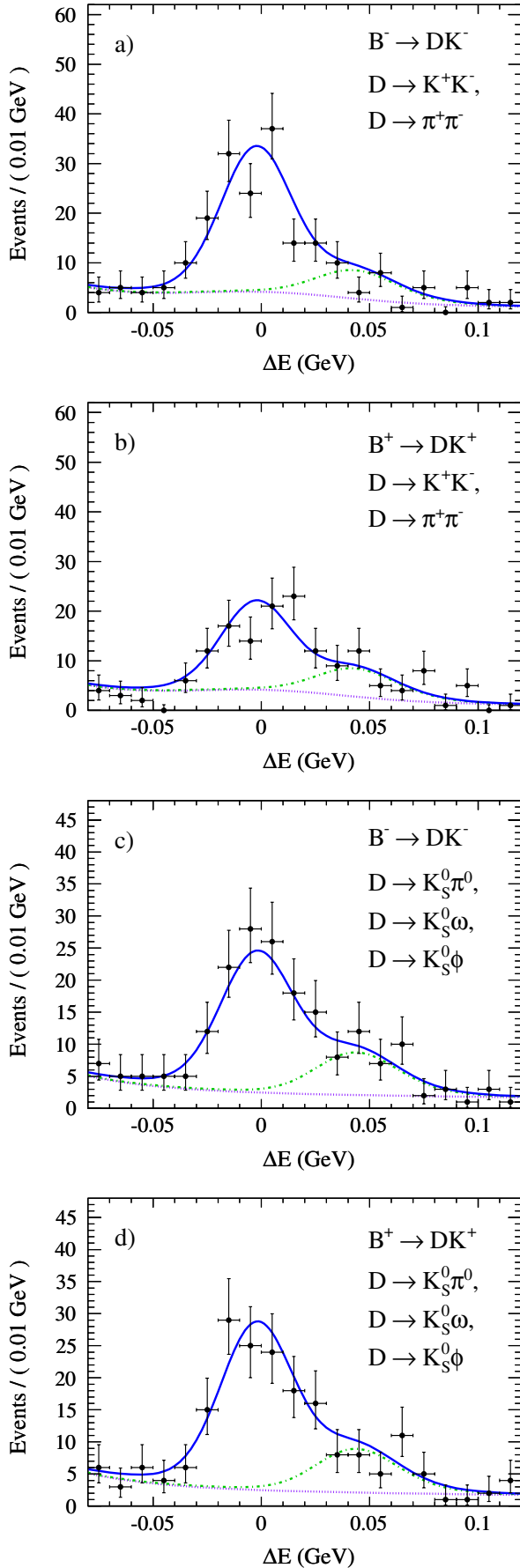
associated systematic uncertainties to be half the size of the bias corrections, summed in quadrature with the statistical uncertainties on the biases. The latter are due to the limited number of test fits used to estimate the corrections.

We investigate a potential charge asymmetry of the *BABAR* detector, due to a possible charge bias in tracking efficiency (e.g. K^+ vs K^-) and/or particle identification. Our analysis includes a number of control samples, in which the *CP* asymmetry is expected to be negligible: the six $B^\pm \to D\pi^\pm$ samples and the $B^\pm \to DK^\pm$ flavor mode ($D \to K\pi$). The weighted average of the charge asymmetry in the control samples is $(-0.95 \pm 0.44)\%$, from which we assign uncertainties of 1.4% to both A_{CP+} and A_{CP-}. We consider these uncertainties to be 100% correlated.

The measured *CP* asymmetry in $B^\pm \to DK^\pm$, $D \to K_S^0\phi$, can be diluted by the presence of $B^\pm \to DK^\pm$ decays followed by D decays to the same final state $K_S^0 K^+ K^-$ as the signal but with opposite *CP* content, such as $D \to K_S^0 a_0$, $a_0 \to K^+ K^-$. The same can happen in the $B^\pm \to DK^\pm$, $D \to K_S^0\omega$ analysis with backgrounds from $B^\pm \to DK^\pm$, $D \to K_S^0\pi^-\pi^+\pi^0$. This background can also affect the ratios R_{CP-}. It is possible to obtain correction factors to both A_{CP-} and R_{CP-} from a fit to the distributions of the relevant helicity angles, $\cos\theta_N$ and $\cos\theta_H$ for $K_S^0\omega$ and $K_S^0\phi$, respectively. The fit is performed on dedicated $B^\pm \to D\pi^\pm$ samples, in which the selection requirements on the helicity angles have not been applied. It can be shown [29] that for these two final states the observed charge asymmetries and ratios should be corrected by a factor

$$A_{CP}^{\text{true}} = A_{CP}^{\text{obs}} \cdot \frac{1 + f_\epsilon |z|^2 R'}{1 - f_\epsilon |z|^2}, \tag{27}$$

$$R_{K/\pi}^{\text{true}} = R_{K/\pi}^{\text{obs}} \cdot \frac{1 + f_\epsilon |z|^2}{1 + f_\epsilon |z|^2 R'}. \tag{28}$$

Here, R' is the ratio of the $R_{K/\pi}^\pm$ values, where $R_{K/\pi}^-$ is taken from a single fit to the $D^0 \to K_S^0\pi^0$ final state only (as opposed to using all three *CP*− final states under study), $R' = R_{K/\pi}^+ / R_{K/\pi}^{K_S^0\pi^0}$, and $f_\epsilon = \epsilon_{\text{sig}}/\epsilon_{\text{bkg}}$ is the ratio of the efficiencies of the selection criterion on the helicity

FIG. 2 (color online). ΔE projections of the fits to the data, split into subsets of definite *CP* of the D candidate and charge of the B candidate: (a) $B^- \to D_{CP+}K^-$, (b) $B^+ \to D_{CP+}K^+$, (c) $B^- \to D_{CP-}K^-$, (d) $B^+ \to D_{CP-}K^+$. The curves are the full PDF (solid, blue), and $B \to D\pi$ (dash-dotted, green) stacked on the remaining backgrounds (dotted, purple). The region between the solid and the dash-dotted lines represents the $B \to DK$ contribution. We show the subsets of the data sample in which the track h from the B decay is identified as a kaon. We require candidates to lie inside the signal-enriched region defined in Sec. IV, except for the plotted variable.
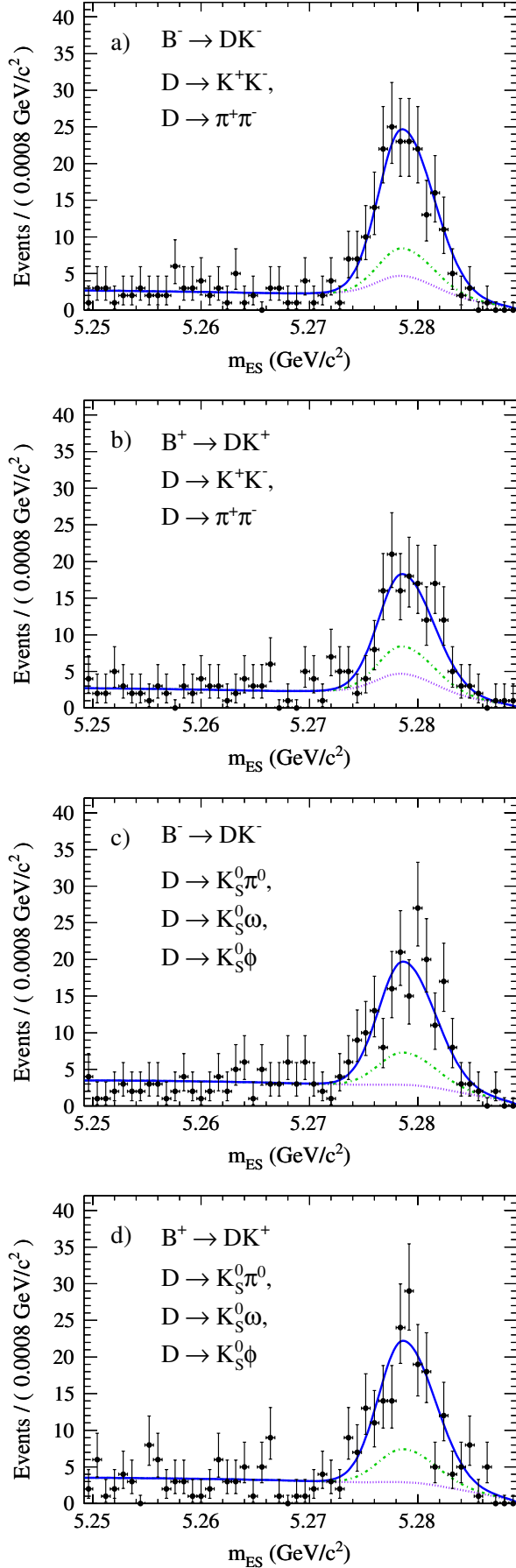
angles: $f_{\epsilon,K_S^0\omega} = 0.71$ and $f_{\epsilon,K_S^0\phi} = 0.64$. To apply these corrections, we first perform a fit of the $K_S^0\pi^0$ final state alone to obtain $R_{K/\pi}^{K_S^0\pi^0}$. We then perform the simultaneous fit of the $CP+$ final states, from which we take the value of $R_{K/\pi}^+$. Finally, we include the correction factors into the $CP-$ final PDF, which will allow the likelihood fitter to correctly estimate their influence. The parameter $|z|^2$ in Eqs. (27) and (28) is extracted from fits of the helicity angle distributions in the $D^0 \to K_S^0\omega$ and $D^0 \to K_S^0\phi$ subsamples to the function $|z|^2 + 3\cos^2\theta$ [29]. We subtract the background expected from the Monte Carlo simulation, which has been rescaled to match the data. We find $|z|^2 = 0.065 \pm 0.033$ in the case of $K_S^0\omega$, and $|z|^2 = 0.217 \pm 0.063$ in the case of $K_S^0\phi$. The uncertainties contain propagated uncertainties due to the background subtraction. The resulting corrections are

$$A_{CP(K_S^0\omega)}^{\text{true}} = A_{CP(K_S^0\omega)}^{\text{obs}} \times (1.105 \pm 0.056), \qquad (29)$$

$$A_{CP(K_S^0\phi)}^{\text{true}} = A_{CP(K_S^0\phi)}^{\text{obs}} \times (1.35 \pm 0.12), \qquad (30)$$

$$R_{K/\pi(K_S^0\omega)}^{\text{true}} = R_{K/\pi(K_S^0\omega)}^{\text{obs}} \times (0.9929 \pm 0.0066), \qquad (31)$$

$$R_{K/\pi(K_S^0\phi)}^{\text{true}} = R_{K/\pi(K_S^0\phi)}^{\text{obs}} \times (0.981 \pm 0.016). \qquad (32)$$

In order to assign systematic uncertainties, we propagate the uncertainties on the correction factors into the final result.

When calculating R_{CP} through Eq. (5) one has to take into account that this equation is an approximation. We define the double ratios used to approximate $R_{CP\pm}$ as $R_\pm$. They are given by

$$R_\pm = \frac{\Gamma(B^- \to D_{CP\pm}K^-) + \Gamma(B^+ \to D_{CP\pm}K^+)}{\Gamma(B^- \to D_f K^-) + \Gamma(B^+ \to \bar{D}_f K^+)}$$
$$\times \frac{\Gamma(B^- \to D_f \pi^-) + \Gamma(B^+ \to \bar{D}_f \pi^+)}{\Gamma(B^- \to D_{CP\pm}\pi^-) + \Gamma(B^+ \to D_{CP\pm}\pi^+)},$$
$$(33)$$

where D_f denotes the $K^-\pi^+$ final state. These can be written as

FIG. 3 (color online). m_{ES} projections of the fits to the data, split into subsets of definite CP of the D candidate and charge of the B candidate: (a) $B^- \to D_{CP+}K^-$, (b) $B^+ \to D_{CP+}K^+$, (c) $B^- \to D_{CP-}K^-$, (d) $B^+ \to D_{CP-}K^+$. We show the subsets of the data sample in which the track h from the B decay is identified as a kaon. See caption of Fig. 2 for line definitions. Only a subrange of the whole fit range is shown in order to provide a closer view of the signal peak.

$$R_{\pm} = \frac{1 + r_B^2 \pm 2r_B \cos\delta_B \cos\gamma}{1 + r_B^2 r_D^2 + 2r_B r_D \cos(\delta_B - \delta_D) \cos\gamma}$$
$$\times \frac{1 + r_{B\pi}^2 r_D^2 + 2r_{B\pi} r_D \cos(\delta_{B\pi} - \delta_D) \cos\gamma}{1 + r_{B\pi}^2 \pm 2r_{B\pi} \cos\delta_{B\pi} \cos\gamma},$$

(34)

where $r_{B\pi}$ and $\delta_{B\pi}$ are defined, in analogy to r_B and δ_B, as $r_{B\pi} e^{i(\delta_{B\pi} - \gamma)} = A(B^- \rightarrow \bar{D}^0 \pi^-)/A(B^- \rightarrow D^0 \pi^-)$, while r_D and δ_D are defined as $r_D e^{i\delta_D} = A(\bar{D}^0 \rightarrow K^- \pi^+)/A(D^0 \rightarrow K^- \pi^+)$. We write Eq. (34) in the form $R_{\pm} = R_{CP\pm} \times (1 + R_c)$, and we assign a relative systematic uncertainty based on the value of the correction R_c. Taking $\sin\theta_C = 0.2257 \pm 0.0010$ (where θ_C is the Cabibbo angle) and $r_B = 0.104^{+0.015}_{-0.025}$ from [3], and expressing $r_D = |V_{cd} V_{us}|/|V_{ud} V_{cs}| = \tan^2\theta_C$, and $r_{B\pi} = r_B \tan^2\theta_C$, we find $R_c \approx 4r_B \tan^2\theta_C \approx 2.2\%$. Here, we have conservatively assumed values for the cosine terms which maximize R_c. We thus assign a relative uncertainty of 2.2% to the values of R_{CP}, fully correlated between R_{CP+} and R_{CP-}.

We also consider the influence on the measured value of A_{CP} of misreconstructed signal B candidates, i.e. candidates reconstructed, in events containing a true $B \rightarrow DK$ decay with D decaying to the same final state X as the reconstructed candidate, from random combinations of particles produced in the true $B \rightarrow DK$ decay and the particles of the ROE. The fraction of these candidates ranges from 0.3% to 12% in simulated $B^{\pm} \rightarrow D_{CP}K^{\pm}$ events, depending on the channel. Since we treat this component like the signal, we implicitly assume that its charge asymmetry is equal to the asymmetry in the signal component. We use simulated signal events to estimate the ratio between misreconstructed and true $B^+ \rightarrow DK^+$ candidates and the ratio between misreconstructed and true $B^- \rightarrow DK^-$ candidates, and find these two quantities to differ by less than 0.1%, from which we derive an upper limit on the difference between the observed and the true value of A_{CP}.

The yield double ratios $R_{CP\pm}$ should be corrected by the corresponding double ratio of selection efficiencies. We find from simulated events that the efficiency double ratios are compatible with each other, and their average value is very close to unity, $(99.46 \pm 0.23)\%$. Thus we do not correct the central values but conservatively assign a relative uncertainty equal to $1 - (0.9946 - 0.0023) = 0.0077$.

The final PDF does not contain an explicit description of the conditional parameter ΔE_{shift}, assuming implicitly that the distribution of ΔE_{shift} observed in data is the same for all the components of the fit. However, the distributions are found to be slightly different across the components, thus introducing a possible bias in the fit results. To estimate the size of this bias, we use simulated events to obtain parametrizations of the ΔE_{shift} distributions of all the fit components and repeat the fits to data. We assign the differences compared to the results of the nomi-
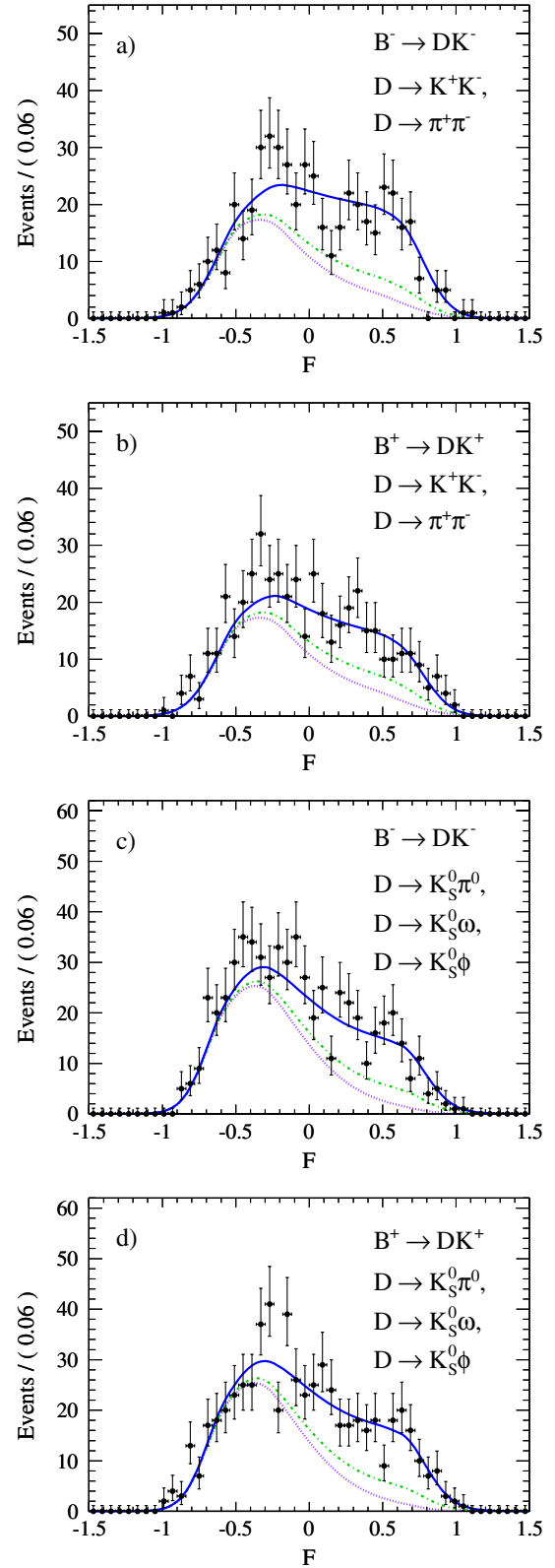

FIG. 4 (color online). $\mathcal{F}$ projections of the fits to the data, split into subsets of definite *CP* of the *D* candidate and charge of the *B* candidate: (a) $B^- \rightarrow D_{CP+}K^-$, (b) $B^+ \rightarrow D_{CP+}K^+$, (c) $B^- \rightarrow D_{CP-}K^-$, (d) $B^+ \rightarrow D_{CP-}K^+$. We show the subsets of the data sample in which the track *h* from the *B* decay is identified as a kaon. See caption of Fig. 2 for line definitions.

nal fits as the systematic uncertainty. We expect this effect to be highly correlated between A_{CP} parameters, because the PDFs are similar in each D decay channel. Thus they are affected by nonuniform $\Delta E_{\texttt{shift}}$ distributions in a similar way. The same argument holds for the $R_{K/\pi}$ parameters. We studied the effect of assigning a 0%, 50%, and 100% correlation. The uncorrelated case gave the largest deviations from the nominal results, the fully correlated case gave the smallest. However, the variation was found to be at the 10% level. We assign the systematic uncertainty corresponding to a correlation of 50%.

Table V lists the contributions of the effects discussed above. Compared to our previous analysis [9], the systematic uncertainty on A_{CP+} is reduced due to better understanding of the detector intrinsic charge asymmetry (the determination of which benefits from the larger data set) and due to improved evaluation of the correlations among the different sources of systematic uncertainties. The uncertainty on A_{CP-} is only slightly reduced. By contrast, the systematic uncertainties on $R_{CP\pm}$ are increased due to two additional sources of uncertainty that were not considered previously: the bias correction and the differences of the $\Delta E_{\texttt{shift}}$ distributions among the fit components. The systematic correlations between the GLW parameters $\vec{y} = (A_{CP+}, A_{CP-}, R_{CP+}, R_{CP-})^T$ are

$$C_{(\text{syst})}[\vec{y}] = \begin{pmatrix} 1 & 0.56 & -0.06 & 0 \\ & 1 & 0 & 0 \\ & & 1 & 0.13 \\ & & & 1 \end{pmatrix}. \quad (35)$$

VIII. RESULTS

The signal yields returned from the fit for each of the D decay modes under study are listed in Table VI. We reconstruct almost 1000 $B^{\pm} \to D_{CP}K^{\pm}$ decays and about 4 times more $B^{\pm} \to DK^{\pm}$, $D \to K\pi$ decays.

The final values of the GLW parameters that we measure are

$$A_{CP+} = 0.25 \pm 0.06(\text{stat}) \pm 0.02(\text{syst}), \quad (36)$$

$$A_{CP-} = -0.09 \pm 0.07(\text{stat}) \pm 0.02(\text{syst}), \quad (37)$$

$$R_{CP+} = 1.18 \pm 0.09(\text{stat}) \pm 0.05(\text{syst}), \quad (38)$$

$$R_{CP-} = 1.07 \pm 0.08(\text{stat}) \pm 0.04(\text{syst}). \quad (39)$$

The statistical correlations among these four quantities are

$$C_{(\text{stat})}[\vec{y}] = \begin{pmatrix} 1 & 0 & -0.08 & 0 \\ & 1 & 0 & 0.03 \\ & & 1 & 0.10 \\ & & & 1 \end{pmatrix}. \quad (40)$$

The results are in good agreement with those from our previous analysis [9] and the current world averages [21].

Figure 2 shows the ΔE projections of the final fits to the CP subsamples and Figs. 3–5 show m_{ES} and $\mathcal{F}$ projections as well as projections of the fit to the $D^0 \to K^-\pi^+$ flavor mode.

The statistical significance of a nonzero A_{CP+} value is determined from the maximum value of the likelihood function of the nominal fit and that of a dedicated null-hypothesis fit, where A_{CP+} was fixed to zero,

$$S_{\text{stat}} = \sqrt{2\ln(\mathcal{L}_{\text{nom}}/\mathcal{L}_{\text{null}})} = 3.7. \quad (41)$$

Taking into account systematic uncertainties, the statistical significance of A_{CP+} is slightly decreased to
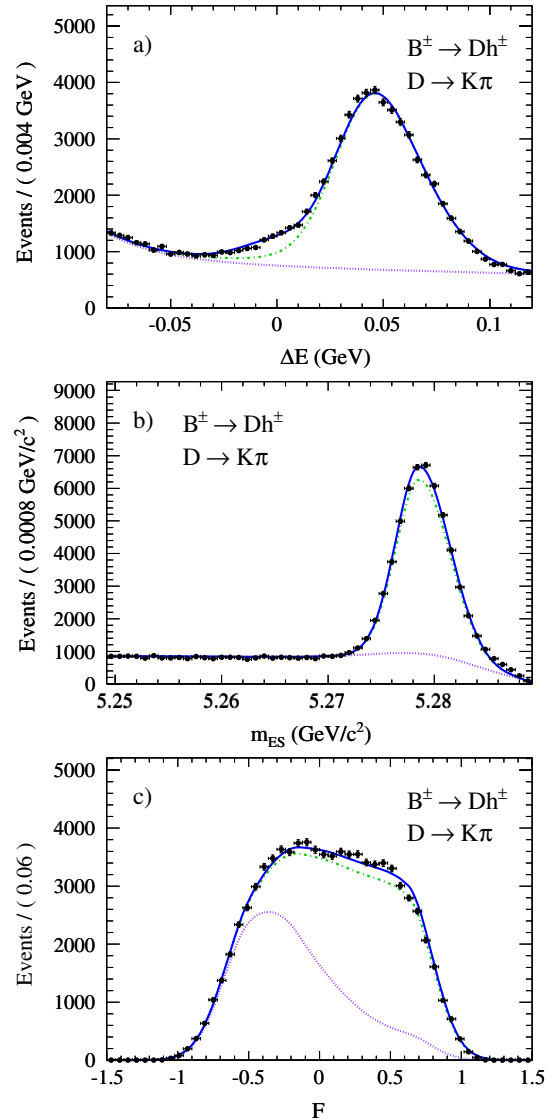

FIG. 5 (color online). Projections of (a) ΔE, (b) m_{ES}, and (c) $\mathcal{F}$ variables of the fit to the $B^{\pm} \to Dh^{\pm}$, $D^0 \to K^-\pi^+$ flavor mode. No requirements are put on the PID of the track h from the B decay and on the fit variables not plotted. See caption of Fig. 2 for line definitions.

$$S_{\text{stat+syst}} = \frac{S_{\text{stat}}}{\sqrt{1 + \frac{\sigma_{\text{syst}}^2}{\sigma_{\text{stat}}^2}}} = 3.6. \qquad (42)$$

This constitutes evidence for direct *CP* violation in charged *B* decays and the first evidence of direct *CP* violation in $B \to DK$.

We constrain the CKM angle γ, the strong phase δ_B, and the amplitude ratio r_B from the present measurement by adopting the frequentist procedure also exploited in [15]. We define a multivariate Gaussian likelihood function

$$\mathcal{L}(\gamma, \delta_B, r_B) = \frac{1}{N} \exp\left(-\frac{1}{2}(\vec{y} - \vec{y}_t)^T V_{\text{cov}}^{-1}(\vec{y} - \vec{y}_t)\right) \quad (43)$$

relating the experimentally measured observables $\vec{y}$ and their statistical and systematic covariance matrices $V_{\text{cov}} = V_{\text{stat}} + V_{\text{syst}}$ with the corresponding truth parameters $\vec{y}_t = \vec{y}_t(\gamma, \delta_B, r_B)$ calculated using Eqs. (3) and (4). The matrices V_{stat} and V_{syst} are constructed from Eqs. (35)–(40). The normalization is $N = (2\pi)^2 \sqrt{|V_{\text{cov}}|}$. We then define a χ^2-function as

$$\chi^2(\gamma, \delta_B, r_B) = -2\ln\mathcal{L}(\gamma, \delta_B, r_B). \qquad (44)$$

Because of the inherent eight-fold ambiguity of the GLW method there are eight equivalent minima of the χ^2-function, χ_{min}^2, which correspond to the same value of r_B and to eight alternative solutions for (γ, δ_B). To evaluate the confidence level of a certain truth parameter (for example γ) at a certain value (γ_0) we consider the value of the χ^2-function at the new minimum, $\chi_{\text{min}}^2(\gamma_0, \delta'_B, r'_B)$, satisfying $\Delta\chi^2 = \chi_{\text{min}}^2(\gamma_0, \delta'_B, r'_B) - \chi_{\text{min}}^2 \geq 0$. In a purely Gaussian situation for the truth parameters the CL is given by the probability that $\Delta\chi^2$ is exceeded for a χ^2-distribution with one degree of freedom:

$$1\text{-CL} = \frac{1}{\sqrt{2}\Gamma(1/2)} \int_{\Delta\chi^2}^{\infty} e^{-t/2} t^{-1/2} dt. \qquad (45)$$

A more accurate approach is to take into account the nonlinearity of the GLW relations, Eqs. (3) and (4). In this case one should consider $\Delta\chi^2$ as a test statistic, and calculate (1-CL) by means of a Monte Carlo procedure, described in the following. For a certain value of interest (γ_0), we

(i) calculate $\Delta\chi^2 = \chi_{\text{min}}^2(\gamma_0, \delta'_B, r'_B) - \chi_{\text{min}}^2$ as before; generate a "toy" result $A'_{CP\pm}$, $R'_{CP\pm}$, using Eq. (43) with values γ_0, δ'_B, r'_B as the PDF;
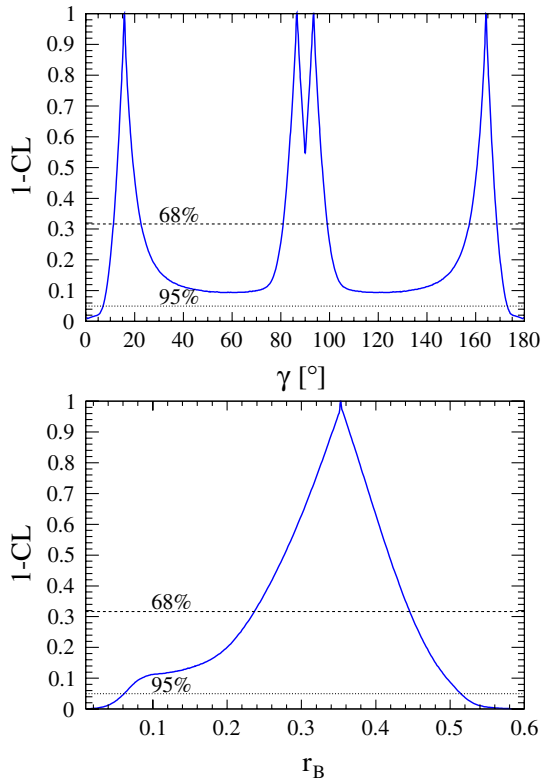

FIG. 6 (color online). 1-CL as a function of γ (top) and r_B (bottom). Both statistical and systematic uncertainties are taken into account. For the angle γ, the plot is identical in the range [180°, 360°]. The horizontal lines show the 68% CL (dashed) and the 95% CL (dotted). Because of the symmetry of Eqs. (3) and (4) the plot for the strong phase δ_B is identical to the one for γ.
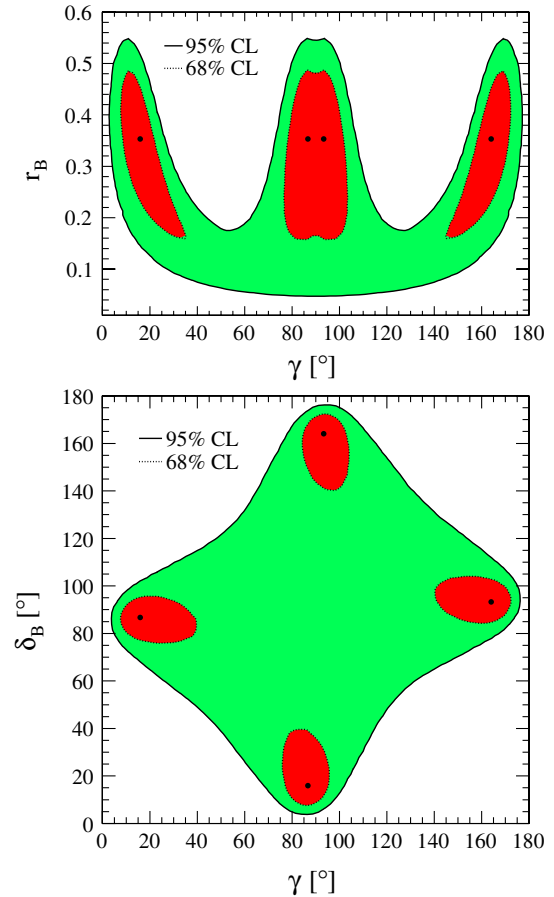

FIG. 7 (color online). Contours at 68% (dotted, red) and 95% (solid, green) 2-dimensional CL in the (γ, r_B) and (γ, δ_B) planes. See also the caption of Fig. 6 regarding symmetries.

TABLE VII. 68% and 95% CL intervals for the parameters γ, and r_B, taking into account both statistical and systematic uncertainties. The confidence intervals for δ_B are identical to those for γ due to the intrinsic $\gamma \leftrightarrow \delta_B$ ambiguity of the GLW method.

	γ mod 180 [°]	r_B
68% CL	[11.3, 22.7]	[0.24, 0.45]
	[80.8, 99.2]	
	[157.3, 168.7]	
95% CL	[7.0, 173.0]	[0.06, 0.51]

   (ii) calculate $\Delta\chi^{2\prime}$ of the toy result as in the first step, i.e. minimize again with respect to δ_B and r_B;
   (iii) calculate (1-CL) as the fraction of toy results which perform better than the measured data, i.e. $1\text{-CL} = N(\Delta\chi^2 > \Delta\chi^{2\prime})/N_{\text{toy}}$.

Figs. 6 and 7 illustrate 1-CL as a function of γ and r_B as obtained from this study. From these distributions we extract 68% and 95% CL confidence intervals for γ and r_B, as summarized in Table VII. Because of the $\gamma \leftrightarrow \delta_B$ ambiguity of the GLW method, the 1D CL intervals for δ_B are identical to those for γ. At the 68% CL we are able to distinguish six out of eight solutions for γ (and δ_B), two of which are in good agreement with the current world averages [25]. At the 95% CL we are able to exclude the

intervals [0°, 7.0°], [173.0°, 187.0°] and [353.0°, 360°] for γ and δ_B. For r_B we deduce at 68% CL:

$$r_B = 0.35^{+0.10}_{-0.11}(\text{stat} + \text{syst}). \qquad (46)$$

In order to facilitate the future combination of these measurements with the results of the Dalitz plot analysis of $B^{\pm} \to DK^{\pm}$, $D \to K_S^0 h^+ h^-$ decays ($h = \pi, K$) [16], we recompute the GLW parameters after excluding from the nominal fit the $D_{CP-} \to K_S^0\phi$ ($\phi \to K^+K^-$) subsample. The sample obtained in this way is statistically independent of that selected in [16]. The final values of the GLW parameters that we measure in this case are

$$A_{CP+} = 0.25 \pm 0.06(\text{stat}) \pm 0.02(\text{syst}), \qquad (47)$$

$$A_{CP-} = -0.08 \pm 0.07(\text{stat}) \pm 0.02(\text{syst}), \qquad (48)$$

$$R_{CP+} = 1.18 \pm 0.09(\text{stat}) \pm 0.05(\text{syst}), \qquad (49)$$

$$R_{CP-} = 1.03 \pm 0.09(\text{stat}) \pm 0.04(\text{syst}). \qquad (50)$$

The statistical correlations among these four quantities are

$$C_{(\text{stat})}[\vec{y}] = \begin{pmatrix} 1 & 0 & -0.08 & 0 \\ & 1 & 0 & 0.04 \\ & & 1 & 0.09 \\ & & & 1 \end{pmatrix}, \qquad (51)$$

and the systematic correlations are

TABLE VIII. Fit result of the three final fits to data, before correcting for fit biases (see Sec. VII).

Parameter	KK	$\pi\pi$	$K_S^0\pi^0$	$K_S^0\omega$	$K_S^0\phi$	$K\pi$
$A_{CP}^{\text{sig}(K)}$	0.242 ± 0.065			−0.089 ± 0.066		−0.008 ± 0.022
$A_{CP}^{\text{sig}(\pi)}$	0.003 ± 0.015			−0.009 ± 0.014		−0.0116 ± 0.0050
$R_{K/\pi}$	0.0897 ± 0.0063			0.0808 ± 0.0056		0.0753 ± 0.0018
m	0.0204 ± 0.0030			0.0206 ± 0.0029		0.02143 ± 0.00089
$A_{CP,f}^{B\bar{B}}$	−0.004 ± 0.045	−0.043 ± 0.047	n/a	n/a	n/a	−0.043 ± 0.017
$A_{CP,p}^{q\bar{q}}$	0.012 ± 0.016	−0.016 ± 0.018	−0.002 ± 0.011	0.012 ± 0.020	−0.069 ± 0.060	−0.027 ± 0.016
$A_{CP,f}^{q\bar{q}}$	−0.004 ± 0.011	−0.0044 ± 0.0098	0.0021 ± 0.0071	−0.004 ± 0.013	0.001 ± 0.039	−0.0016 ± 0.0068
$f_{\mathcal{F}}^{q\bar{q}}$	0.326 ± 0.026	0.49 (fixed)	0.520 ± 0.030	0.27 (fixed)	n/a	0.396 ± 0.018
$\sigma_{\mathcal{F},l,1}^{q\bar{q}}$	0.160 ± 0.016	0.258 ± 0.023	0.206 ± 0.014	0.175 ± 0.034	0.2758 ± 0.0092	0.198 ± 0.014
$\sigma_{\mathcal{F},l,2}^{q\bar{q}}$	0.1742 ± 0.0020	0.2047 ± 0.0024	0.1546 ± 0.0015	0.1963 ± 0.0028	n/a	0.1965 ± 0.0017
$\sigma_{\mathcal{F},r,1}^{q\bar{q}}$	0.312 ± 0.011	0.329 ± 0.011	0.3541 ± 0.0068	0.317 ± 0.019	0.447 ± 0.014	0.3068 ± 0.0061
$\sigma_{\mathcal{F},r,2}^{q\bar{q}}$	0.231 ± 0.014	0.268 ± 0.018	0.275 ± 0.020	0.238 ± 0.013	n/a	0.237 ± 0.010
$\sigma_{\Delta E,m_{ES}}^{B\bar{B}}$	n/a	n/a	n/a	n/a	n/a	0.01048 ± 0.00057
$a_{\Delta E}^{q\bar{q}}$	−0.96 ± 0.14	−0.71 ± 0.14	−0.924 ± 0.099	−1.04 ± 0.18	−0.48 (fixed)	−0.88 ± 0.10
$\mu_{\Delta E}$	−2.62 ± 0.32	−1.36 ± 0.57	−1.80 ± 0.35	−2.87 ± 0.59	−0.95 ± 0.75	−1.527 ± 0.092
$\sigma_{\Delta E}$	16.63 ± 0.27	14.82 ± 0.49	17.01 ± 0.29	16.10 ± 0.52	15.82 ± 0.60	15.424 ± 0.076
$\mu_{m_{ES}}$	5278.56 ± 0.12	5278.61 ± 0.20	5278.62 ± 0.12	5278.50 ± 0.22	5278.99 ± 0.25	5278.586 ± 0.033
$\sigma_{m_{ES},l}$	2.207 ± 0.081	2.12 ± 0.15	2.299 ± 0.084	2.11 ± 0.16	2.33 ± 0.17	2.210 ± 0.022
$\sigma_{m_{ES},r}$	2.897 ± 0.081	2.83 ± 0.15	2.922 ± 0.084	3.08 ± 0.16	2.72 ± 0.17	2.852 ± 0.023
$N_p^{B\bar{B}}$	79 ± 29	346 ± 52	176 ± 43	180 ± 48	3 (fixed)	328 ± 40
$N_f^{B\bar{B}}$	1430 ± 82	1517 ± 142	1930 ± 102	1195 ± 109	119 ± 20	7717 ± 170
$N_p^{q\bar{q}}$	4005 ± 69	3456 ± 76	8587 ± 101	2675 ± 68	284 ± 17	4722 ± 77
$N_f^{q\bar{q}}$	10890 ± 125	13019 ± 176	21657 ± 172	6673 ± 124	716 ± 29	28007 ± 205
$N_{\text{tot}}^{\text{sig}(\pi)}$	4091 ± 70	1230 ± 41	4182 ± 73	1440 ± 45	648 ± 27	44631 ± 232

$$C_{(\text{syst})}[\vec{y}] = \begin{pmatrix} 1 & 0.56 & -0.06 & 0 \\ & 1 & 0 & 0 \\ & & 1 & 0.12 \\ & & & 1 \end{pmatrix}. \quad (52)$$

To compare the results obtained after removing the $D_{CP-} \to K_S^0 \phi$ subsample with those from the $B^\pm \to DK^\pm$, $D \to K_S^0 h^+ h^-$ analyses, which are expressed in terms of the variables $x_\pm = r_B \cos(\delta_B \pm \gamma)$ and $y_\pm = r_B \sin(\delta_B \pm \gamma)$, we use the GLW parameters measured in this way to determine the quantities $x_\pm$ through the relations:

$$x_\pm = \frac{1}{4}[R_{CP+}(1 \mp A_{CP+}) - R_{CP-}(1 \mp A_{CP-})]. \quad (53)$$

We obtain

$$x_+ = -0.057 \pm 0.039(\text{stat}) \pm 0.015(\text{syst}), \quad (54)$$

$$x_- = 0.132 \pm 0.042(\text{stat}) \pm 0.018(\text{syst}). \quad (55)$$

These results are in good agreement with the current world averages [21] and have precision close to the single most precise measurements [16]. We also measure r_B^2, which provides a constraint on $x_\pm$ and $y_\pm$ via $r_B^2 = x_\pm^2 + y_\pm^2$, from

$$r_B^2 = \frac{1}{2}(R_{CP+} + R_{CP-} - 2). \quad (56)$$

We determine:

$$r_B^2 = 0.105 \pm 0.067(\text{stat}) \pm 0.035(\text{syst}). \quad (57)$$

The constraints that could be placed on the quantities $y_\pm$ from these measurements, by exploiting the relation $r_B^2 = x_\pm^2 \pm y_\pm^2$, are much weaker than those provided by the $B^\pm \to DK^\pm$, $D \to K_S^0 h^+ h^-$ analysis.

As a final check of consistency we consider the quantity a,

$$a = A_{CP+}R_{CP+} + A_{CP-}R_{CP-}. \quad (58)$$

From Eqs. (3) and (4) one expects a to satisfy $a = 0$. We measure $a = 0.19 \pm 0.11(\text{stat} + \text{syst})$, which is compatible with 0.

IX. SUMMARY

Using the entire data set collected by *BABAR* at the e^+e^- center-of-mass energy close to the $\Upsilon(4S)$ mass, we have reconstructed $B^\pm \to DK^\pm$ decays, with D mesons decaying to non-*CP* ($K\pi$), *CP*-even (K^+K^-, $\pi^+\pi^-$) and *CP*-odd ($K_S^0\pi^0$, $K_S^0\phi$, $K_S^0\omega$) eigenstates.

Through an improved analysis method compared to the previous *BABAR* measurement [9] and through an enlarged data set, corresponding to an increase in integrated luminosity at the $\Upsilon(4S)$ peak from 348 fb^{-1} to 426 fb^{-1}, we obtain the most precise measurements of the GLW parameters $A_{CP\pm}$ and $R_{CP\pm}$ to date:

$$A_{CP+} = 0.25 \pm 0.06(\text{stat}) \pm 0.02(\text{syst}),$$

$$A_{CP-} = -0.09 \pm 0.07(\text{stat}) \pm 0.02(\text{syst}),$$

$$R_{CP+} = 1.18 \pm 0.09(\text{stat}) \pm 0.05(\text{syst}),$$

$$R_{CP-} = 1.07 \pm 0.08(\text{stat}) \pm 0.04(\text{syst}).$$

We measure a value of A_{CP+} which is 3.6 standard deviations from zero, which constitutes the first evidence for direct *CP* violation in $B \to DK$ decays.

From the measured values of the GLW parameters, we extract confidence intervals for the CKM angle γ, the strong phase δ_B, and the amplitude ratio r_B, using a frequentist approach, taking into account both statistical and systematic uncertainties. At the 68% CL we find that both γ and δ_B (modulo 180°) belong to one of the three intervals [11.3°, 22.7°], [80.8°, 99.2°] or [157.3°, 168.7°], and that

$$r_B \in [0.24, 0.45].$$

At 95% CL, we exclude the intervals [0°, 7.0°], [173.0°, 187.0°] and [353.0°, 360°] for γ and δ_B, and measure

$$r_B \in [0.06, 0.51].$$

Our results are in agreement with the current world averages [25].

To facilitate the combination of these measurements with the results of our Dalitz plot analysis of $B^\pm \to DK^\pm$, $D \to K_S^0 h^+ h^-$ ($h = K, \pi$) [16], we exclude the $D \to K_S^0 \phi$, $\phi \to K^+K^-$ channel from this analysis—thus removing events selected also in [16]—and then determine

$$A_{CP-} = -0.08 \pm 0.07(\text{stat}) \pm 0.02(\text{syst}),$$

$$R_{CP-} = 1.03 \pm 0.09(\text{stat}) \pm 0.04(\text{syst}).$$

For comparison with the results of the $B^\pm \to DK^\pm$, $D \to K_S^0 h^+ h^-$ analyses, which are expressed in terms of the variables $x_\pm = r_B \cos(\delta_B \pm \gamma)$ and $y_\pm = r_B \sin(\delta_B \pm \gamma)$, we express our results for the GLW observables in terms of x_+ and x_-. We measure

$$x_+ = -0.057 \pm 0.039(\text{stat}) \pm 0.015(\text{syst}),$$

$$x_- = 0.132 \pm 0.042(\text{stat}) \pm 0.018(\text{syst}),$$

at 68% CL. These results are in good agreement with the current world averages [21] and have precision comparable to the single most precise measurements [16]. We also evaluate r_B after the exclusion of the $D \to K_S^0 \phi$ channel, and obtain a weak constraint on $r_B^2 = x_\pm^2 \pm y_\pm^2$:

$$r_B^2 = 0.105 \pm 0.067(\text{stat}) \pm 0.035(\text{syst})$$

at 68% CL.

ACKNOWLEDGMENTS

[1] N. Cabibbo, Phys. Rev. Lett. **10**, 531 (1963).

[2] M. Kobayashi and T. Maskawa, Prog. Theor. Phys. **49**, 652 (1973).

[3] J. Charles *et al.*, Eur. Phys. J. C **41**, 1 (2005), and updates at http://ckmfitter.in2p3.fr.

[4] M. Gronau and D. Wyler, Phys. Lett. B **265**, 172 (1991).

[5] M. Gronau and D. London, Phys. Lett. B **253**, 483 (1991).

[6] D. Atwood, I. Dunietz, and A. Soni, Phys. Rev. Lett. **78**, 3257 (1997).

[7] D. Atwood, I. Dunietz, and A. Soni, Phys. Rev. D **63**, 036005 (2001).

[8] A. Giri, Y. Grossman, A. Soffer, and J. Zupan, Phys. Rev. D **68**, 054018 (2003).

[9] B. Aubert *et al.* (*BABAR* Collaboration), Phys. Rev. D **77**, 111102 (2008).

[10] B. Aubert *et al.* (*BABAR* Collaboration), Phys. Rev. D **78**, 092002 (2008).

[11] B. Aubert *et al.* (*BABAR* Collaboration), Phys. Rev. D **80**, 092001 (2009).

[12] B. Aubert *et al.* (*BABAR* Collaboration), Phys. Rev. D **72**, 032004 (2005).

[13] B. Aubert *et al.* (*BABAR* Collaboration), Phys. Rev. D **76**, 111101(R) (2007).

[14] B. Aubert *et al.* (*BABAR* Collaboration), Phys. Rev. D **80**, 031102(R) (2009).

[15] B. Aubert *et al.* (*BABAR* Collaboration), Phys. Rev. D **78**, 034023 (2008).

[16] B. Aubert *et al.* (*BABAR* Collaboration), Phys. Rev. Lett. **105**, 121801 (2010).

[17] B. Aubert *et al.* (*BABAR* Collaboration), Phys. Rev. D **79**, 072003 (2009).

[18] Y. Grossman, A. Soffer, and J. Zupan, Phys. Rev. D **72**, 031501 (2005).

[19] K. Abe *et al.* (Belle Collaboration), Phys. Rev. D **73**, 051106 (2006).

[20] T. Aaltonen *et al.* (CDF Collaboration), Phys. Rev. D **81**, 031105(R) (2010).

[21] E. Barberio *et al.* (HFAG), arXiv:0808.1297, and updates at http://www.slac.stanford.edu/xorg/hfag.

[22] B. Aubert *et al.* (*BABAR* Collaboration), Nucl. Instrum. Methods Phys. Res., Sect. A **479**, 1 (2002).

[23] S. Agostinelli *et al.* (GEANT4 Collaboration), Nucl. Instrum. Methods Phys. Res., Sect. A **506**, 250 (2003).

[24] D. J. Lange, Nucl. Instrum. Methods Phys. Res., Sect. A **462**, 152 (2001).

[25] C. Amsler *et al.* (Particle Data Group), Phys. Lett. B **667**, 1 (2008), and updates at http://pdg.lbl.gov.

[26] G. C. Fox and S. Wolfram, Phys. Rev. Lett. **41**, 1581 (1978).

[27] M. J. Oreglia, Ph.D. thesis, SLAC-R-236, Stanford University, 1980, Appendix D.

[28] H. Albrecht *et al.* (ARGUS Collaboration), Phys. Lett. B **241**, 278 (1990).

[29] G. Marchiori, Ph.D. thesis, SLAC-R-947, Università degli Studi Di Pisa, 2005.